Hirsch, K. K., Scheck-Wenderoth, M., van Wees, J.-D., Kuhlmann, G. (2010): Tectonic subsidence history and thermal evolution of the Orange Basin. - Marine and Petroleum Geology, 27, 3, 565-584

DOI: 10.1016/j.marpetgeo.2009.06.009

Tectonic subsidence history and thermal evolution of the Orange Basin

Katja K. Hirsch[1], Magdalena Scheck-Wenderoth[2], Jan-Diederik van Wees[3], Gesa Kuhlmann[4]

[1]Helmholtz-Zentrum Potsdam Deutsches GeoForschungsZentrum - GFZ, Telegrafenberg, 14473 Potsdam, Germany: hirsch@gfz-potsdam.de, Fax: +49 -331-288-1349 (corresponding author)

[2]Helmholtz-Zentrum Potsdam Deutsches GeoForschungsZentrum - GFZ, Telegrafenberg, 14473 Potsdam, Germany: leni@gfz-potsdam.de, Fax: +49 -331-288-1349

[3]TNO-NITG, division Geo-Energy, Postbus 80015, 3508 TA Utrecht, The Netherlands: Jan_Diederik.vanWees@tno.nl

[4]Helmholtz-Zentrum Potsdam Deutsches GeoForschungsZentrum - GFZ, Telegrafenberg, 14473 Potsdam, Germany: kuhlmann@gfz-potsdam.de, Fax: +49 -331-288-1436

Abstract

The Orange Basin offshore southwest Africa appears to represent a classical example of continental rifting and break up associated with large-scale, transient volcanism. The presence of lower crustal bodies of high seismic velocities indicates that large volumes of igneous crust formed as a consequence of lithospheric extension.

We present results of a combined approach using subsidence analysis and basin history inversion models. Our results show that a classical uniform stretching model does not account for the observed tectonic subsidence. Moreover, we find that the thermal and subsidence implications of underplating need to be considered. Another departure from the uniform stretching model is renewed sub-crustal thinning and linked to that uplift in the Cenozoic that is necessary to reproduce the observed phases of erosion and the present-day depth of the basin. The dimension of these events has been examined and quantified in terms of tectonic uplift and sub-crustal thinning. Based on these forward models we predict the heat flow evolution not only for the available real wells but also for virtual wells over the entire study area. Finally, the hydrocarbon potential and the temperature evolution is presented and shown in combination with inferred maturation of the sediments for depth intervals which comprise potential source rocks.

1 Introduction

Basins located in a passive margin setting are commonly regarded as quiescent after the transition from rift to drift stage and during the following subsidence. Nevertheless, most of these basins may undergo strata disruption to some degree caused by processes such as salt mobilisation, post break up flank uplift or margin instability. The Orange Basin offshore western South Africa (Figure 1) is one of the few examples where these margin deformation mechanisms were not active or dormant throughout most of the basin history. Since the basin contains the stratigraphic record from lithospheric extension and rift tectonics to a fully evolved post-break up setting it provides an ideal area to study the evolution of a “passive”

continental margin. With this study, we aimed on analysing the tectonic history of the Orange Basin.

Though several campaigns have been carried out, with a resultant established seismic and stratigraphic framework for the Orange Basin (e.g. Brown et al., 1995), many aspects and main questions of basin formation and margin evolution remain unexplored. In particular, processes in the underlying mantle and mechanisms for suspected phases of uplift and denudation along the margin are poorly understood.

Here, we develop a tectonic model that explains both the observed subsidence history as well as phases of uplift and erosion while incorporating the observed crustal configuration.

A combined approach of reverse and forward modelling has been applied in the course of which several model configurations have been tested. Classical approaches obeying the principles of uniform stretching (McKenzie, 1978) have been applied and have been further expanded for departures as the effects of underplating and renewed thinning in the mantle. Thermal implications of these departures have been analysed and the respective temperature evolution has been cross-checked with observed vitrinite reflectance data.

2 Database

The database for this study comprises 2D seismic reflection profiles of 6 s TWT recording time and of 2000 km length in total (Figure 1c,2). Tied to these profiles, 7 wells have been investigated that are located on the continental shelf in varying water depths ranging from 240 m to 750 m (Figure 2,3). Wells placed along seismic profiles allowed us to attribute sedimentary lithologies to the interpreted seismic horizons. Age constraints for the interpreted seismic horizons have been provided by the Petroleum Agency South Africa in the form of biostratigraphic picks for the drilled successions. Well data also included gamma-ray wire-line logs, lithologies, and vitrinite reflectance.

These data provided the base for a seismic stratigraphic investigation published by Paton et al. (2008) for which a local seismic stratigraphic nomenclature was used devoted solely to the Orange Basin and developed at the Petroleum Agency of South Africa, former

SOEKOR, (McMillan, 2003) in the 1990s and described by Brown et al. (1995) and Muntingh and Brown (1993).

From the interpretation of seismic data a 3D geological model of the basin infill was created by Hirsch et al. (2007) and used to investigate the underlying lithospheric structure. The crustal configuration for this model was derived using information from deep seismic sounding for 3D gravity modelling. This study yielded the presence of a high density, lower crustal body with a stark density contrast compared to a less dense lower crust continentward. The thickness of this body is used in this study to assess the influence of underplating on the basin´s evolution (Figure 4a).

In summary, we use detailed well information and the previously developed 3D model. The latter not only includes information on the configuration of the sediments but also accounts for the lithologies, porosities and densities of the different layers as well as thermal properties such as radioactive heat production and conductivities.

An additional source of information was a set of vitrinite reflectance data, a widely used indicator for the maturity of organic matter (e.g. Allen and Allen, 2006; Héroux et al., 1979). Vitrinite reflectance increases with increasing burial and temperature, and represents a good measure of the peak paleo temperature to which the sample has been subjected to in its history (Corcoran and Clayton, 2001 and references therein; Dow, 1977). Since thermal reactions are irreversible, vitrinite reflectance data are a reliable thermal calibration method to assess and quantify the denudation (e.g. Allen and Allen, 2006; Burnham and Sweeney, 1989, Dow, 1977). A quantitative assessment of the peak paleo temperatures achieved by potential source rock intervals is decisive for the maturation of the organic matter (Corcoran and Clayton, 2001). Several drawbacks such as the reworking of organic material, identification of primary vitrinite material, rough texture or inclusions should be taken into account but for a depth interval of 1-4 km vitrinite reflectance is a good measure of the maximum paleo temperature and for the evaluation of the thermal alteration of sedimentary rocks (Héroux et al., 1979). Therefore, vitrinite reflectance data are used in this study to cross-check the predicted thermal history of the basin.

3 The Basin

The Orange Basin is situated on the passive continental margin offshore South Africa and southern Namibia (Figure 1). The southern, African continent comprises onshore several geological provinces. The Kalahari Shield, the eldest province, developed approximately 1 Ga ago when ocean-like crust was emplaced over the Kaapvaal Craton (Eglington and Armstrong, 2003). A large network of Proterozoic to early Paleozoic belts established ensuing through the Damara orogeny. Part of this orogeny was the evolution of the Saldanha Belt in South Africa (e.g. Grunow et al., 1996). The history of the continent was tranquil after the cessation of the orogeny and it was dominated by erosion and sedimentation. Until ~250 Ma ago, Cambrian metasediments were extensively deformed into the Cape Fold Belt with complex extensional and compressional structures overlying partly the Saldanha Belt (Hälbich, 1993). The next geological event of regional relevance was the onset of the Mesozoic rifting.

Basin initiation was part of the rifting between South America and Africa that resulted in the break up of the South Atlantic in Early Cretaceous times. Studies along the South African continental margin indicate that the rifting history was complex (Bauer et al., 2000; Gladczenko et al., 1997; Gladczenko et al., 1998; Stewart et al., 2000). It is, however, evident that the continental break up of the continents was accompanied by massive, transient volcanic activity evidenced by the widespread occurrence of volcanic rocks. Coevally to rifting, the South Atlantic Large Igneous Province was emplaced, which encompasses the Paraná–Etendeka continental flood basalts. Offshore, a wedge of seaward dipping reflectors is interpreted to represent the offshore counter part of these extrusive complexes (Bauer et al., 2000; Gladczenko et al., 1997; Hinz, 1981; Hirsch et al., 2007; Talwani and Abreu, 2000). The analysis of volcanic rocks onshore South Africa and Namibia is able to give age constraints on the age of rift initiation as these rocks were emplaced due to the prevailing magmatism at the time of initial extension. The ages of these rocks vary

along the margin between 132 ± 6 Ma (Reid et al., 1991), 134 ± 4 Ma (Reid and Rex, 1994) and ~134 Ma (Seider and Mitchell, 1976).

Offshore Namibia and also farther south, offshore South Africa, deep seismic profiles revealed the presence of a high velocity body in the lower crust which is assumed to be the intrusive counterpart of the seaward dipping reflector wedge found in the distal parts of the Orange Basin. Because of its seismic properties and modelled densities this body is interpreted as an underplated mafic wedge (Bauer et al., 2000; Hirsch et al., in press). Within the working area, the thickness of this body ranges from a few kilometres to up to 13 km (Figure 4a). It is partially responsible for a positive gravity anomaly, the so-called edge-effect anomaly. The marine gravity field in the basin is dominated by this positive, free-air anomaly above the shelf break which commonly is observed along passive continental margins.

Rifting was accompanied by initial faulting and the creation of grabens and half-grabens aligned roughly parallel to the present coastline (Gerrard and Smith, 1982). Where drilled, the syn-rift graben infills were found to consist predominantly of continental sediments (fluvial claystones, sandstones, and pebble beds), volcaniclastics, and volcanics in places (Broad et al. 2006; McMillan, 2003). The fluvial, coarse clastic nature of the syn-rift deposits indicates that deposition started in a mostly continental environment and the preserved thickness of this unit reaches up to 1200 m in places (Figure 4b). A medial hinge zone separates this graben complex from the more distal western wedge of seaward dipping reflectors (Broad et al., 2006). A linear high, the “marginal ridge”, marks the boundary beyond which true oceanic crust occurs (Figure 1b).

The graben infills are overlain by an “end-of-rifting” Hauterivian unconformity (6at1; Figure 2; Gerrard and Smith, 1982; Muntingh and Brown, 1993). The eldest of the three source rock intervals in the Orange Basin developed within the Hauterivian sediments.

Thermal subsidence created the major depocentre which was entered via two points in the area of the present-day Orange and the Olifants River (Figure 1b; Broad et al., 2006) and the basin received the majority of the drainage of Southern Africa from Early Barremian to Late Campanian times (McMillan, 2003; Muntingh and Brown, 1993).

The following upward drift successions are subdivided by unconformities described by Brown et al. (1995) and Muntingh and Brown (1993).

The early drift successions (6at1-13at1, 117.5 -112 Ma) built up a ramp-like sequence on the outer and middle shelf with no distinct shelf-break. The sequence comprises coarsening-upwards predominanty siliclastic, deltaic deposits of areally restricted red beds, marine sandstones and shales (Gerrard and Smith, 1982). The thickness of this unit points to an elongated depocentre with a NNW-SSE trending axis, where a maximum of 1500 m of sediments is preserved (Figure 5a). However, the lithology of this interval appears to vary significantly from north to south. North of the working area, shales rest on gas-bearing sandstones intercalated by basaltic lavas (Gerrard and Smith, 1982). To the contrary, the wells A-C1 and A-C2 encountered mainly sandstones and minor conglomerates and closer inshore, wells intersected continental red beds with minor amounts of lavas or igneous intrusions (Gerrard and Smith, 1982).

In the early and middle Aptian extensive drowning led to the deposition of regional organic-rich petroleum source rocks (Van der Spuy, 2003). The basin expanded shoreward in this time interval when the Barremian to middle Albian successions progressively overstepped the underlying sequences in an eastward direction and sedimentation gave rise to the build-up of a paleo shelf break.

Between the deposition of the Aptian horizon (13at1, 112 Ma) and the Cenomanian/Turonian horizon (15at1, 93 Ma) sedimentation was concentrated on the middle shelf domain where a shelf break of up to 2000 m developed. At the same time, sedimentation was reduced on the inner shelf (Figure 5b). The basin migrated offshore slowly from Middle Albian times on and the thickest portions were deposited until Cenomanian times. In general, sedimentation was more clay-rich than before and included coarsening-upward silts to medium sandstones. Massive sandstones developed locally across the paleo outer shelf.

On the outer margin, the lowermost part of the package comprises the anoxic black shales of Barremian and Aptian age which represent the region’s best source rocks (Herbin et al.,

1987; Paton et al., 2008). Paleontological data document a decreasing water depth which remained shallower than today at all times since Early Aptian times (McMillan, 2003).

A north-westward shift of the depocentre is indicated by the cumulative thickness of the Cenomanian/Turonian (15at1, 93 Ma) to Campanian (18at1, 75 Ma) successions (Figure 5c). Across the inner and middle margin sedimentation deposited packages of moderately uniform thicknesses. The lithologies are fluvial sands and occasional grits, interbedded with shales and occasional silt stringers in varying proportions. In the area of the A-Wells thicknesses of 900 – 1500 m are preserved today. These successions host the most speculative source rock interval of Cenomanian to Turonian age (Paton et al., 2008; Van der Spuy et al., 2003). Faulting affected restricted areas of the slope break.

Heretofore, sedimentation was concentrated on the middle margin but shifted seawards onto the outer margin since Campanian times. A rather thin succession (> 500 m) of deep-water chalks (18at1-22at1, 75-67 Ma) developed on the paleo upper slope (Figure 5d; McMillan, 2003). The outer margin was affected by post-depositional faulting (Paton et al., 2008). In the Latest Cretaceous, in Mid-Campanian, margin tilting and, linked to that, uplift brought sedimentation in the proximal parts of the Orange Basin to an end and let to erosion of the previously deposited successions (McMillan, 2003).

Two horizons are used to give constraints on the timing of the erosional event. First, the youngest horizon (77.5 Ma) found below the erosional unconformity, and second, the horizon 22at1 (67 Ma) which marks the erosional termination. Based on these observations an age of 74 Ma was assigned for the initiation of erosion in our models. Further evidence is provided by the absence of Maastrichtian sediments in the wells on the inner margin in contrast to deposition on the outer margin. Detailed mapping of the unconformity and the concordant nature of reflections were used to reconstruct the horizon´s geometry prior to erosion and to estimate the magnitude of erosion (Figure 6a; Kuhlmann et al., 2008). According to these estimates, a maximum of 280 m of sediments has been eroded close to the coast whereas the amount of erosion is decreasing seawards. Wells A-C3 and A-N1 mark the outer limit of the area affected by erosion.

The horizon 22at1 (67 Ma) defines the base of the Tertiary sedimentary wedge the thickness of which increases from a few hundred metres on the highly stable Cretaceous shelf to 1200 m on the outer shelf (Figure 5e). The preserved thicknesses of these sediments indicate a seaward shift of the main depocentre. Since Tertiary, these strata have been affected by margin instability and gravity faulting. Slumping is common throughout the Cenozoic succession (Faulkner, 2000) due to rejuvenation of older faults expressed in the development of growth faults and toe-thrust systems on the outer margin (Brown et al., 1995; Paton et al., 2008). Claystones and sandstones compose the bulk of the Lower Tertiary successions (Gerrard and Smith, 1982).

Tectonically driven renewed margin uplift led to the establishment of an erosional unconformity in response of which material is only preserved in the proximal deep water domains (McMillan, 2003). Like for the first erosional event, estimates on the amount of erosion have been derived from seismic interpretation and well information (Figure 6b). Seismic interpretation suggests that this second phase of erosion ceased when the deposition of the 14 Ma old Miocene unit started. In the distal domains, west of the shelf break, seismic data image Early Tertiary units cut by the erosional unconformity but no well data are available to calibrate the stratigraphy in detail. As no further constraints were accessible for the onset of erosion, this second, more intensive phase of erosion was assumed to start at 16 Ma and to last until 14 Ma in the course of the modelling.

The Upper Tertiary succession is found to consist of sandy and shelly limestone and calcareous sandstones based on occasional bit samples (Gerrard and Smith, 1982). A thin veneer on top of these successions represents the sedimentation from 14 Ma until recent (Figure 5f).

In the past, the water depths remained always shallow in the basin relative to present-day water depth. The deepening towards the present-day water depth occurred later than Maastrichtian times (McMillan, 2003).

4 Method

A combined approach of subsidence analysis and forward modelling (Van Wees and Beekman, 2000; Van Wees et al., in press) was chosen to gain better insights into the interplay of tectonics and subsidence. Therefore, a 1D analysis of well data was conducted using a two-step procedure: First, a geohistory analysis was carried out for the wells to determine the tectonic subsidence, which is to say, the process of deposition was reversed for each well using a backstripping technique. Second, 1D forward models for lithospheric thinning have been calculated and compared to the tectonic subsidence derived from backstripping. Changes have been successively applied to the forward models until a match between modelled and 'observed' tectonic subsidence was obtained and paleo temperature indicators were reproduced. These changes relate to different mechanisms that may have influenced the subsidence history, such as uniform or depth-dependent thinning and the effects of underplating.

Having obtained a reasonable tectonic history for the 1D case based on real wells, we applied the respective forward scenario to synthetic wells located at the grid points of the 3D structural model. Though a multi-1D approach is applied, the results give a first approximation how the subsidence history varies in 3D and allows predictions for areas without well control.

4.1 Backstripping

The technique of backstripping is commonly applied to extensional basins to determine the magnitude of lithospheric thinning from the observed post-rift subsidence (Sclater and Christie, 1980). Stratigraphic units within a sediment column are removed progressively from top downwards. The remaining sediments are decompacted and isostatically restored using Airy isostasy (Airy, 1855). Thus, the restoration accounts for new load conditions, paleo water depth, and the isostatic response to the change in loads.

Log information is used to compile the lithological composition for each well, within which the fractions of silt, sand, shale, and carbonates were predefined. The reversal of the

compaction process follows a double exponential porosity-depth law (Bond and Kominz, 1984). Therefore, decompaction and its physical impact on density and on thermal conductivity are taken into account (Table1).

The quality of any geohistory analysis is fundamentally dependent upon the quality of paleo water depth information available (e.g. Roberts et al., 1998). The water body provides an additional load contribution to the isostatic response of the system and, in turn, to the observed subsidence. Besides erosional unconformities indicating zero water depth, information concerning paleo water depth usually comes from biostratigraphy. In a global sense, the confidence level for foraminiferal biostratigraphy is unusually high in the basins of the South Atlantic (McMillan, 2003). Paleontological information was kindly provided by the Petroleum Agency of South Africa for the wells used in this study. Well reports document the general depositional environment through time and provide an estimate of paleo water depth. The interpreted chronostratigraphic plot of the Orange Basin provides good information on sea level fluctuations in Cretaceous times on a regional scale (McMillan, 2003). However, Cenozoic uplift of the margin and, linked to that, erosion partially removed the uppermost Cretaceous units. Thus, a reconstructed sea level curve must always remain incomplete for this time interval (McMillan, 2003). For the modelling we use absolute paleo water depth proposed by McMillan (2003).

The output of backstripping comprises basically two subsidence curves. The first one, the basement subsidence, describes the subsidence the basement experienced as documented in the stratigraphy of the well. This curve is a composite of two components: (1) the effects of non-tectonic processes such as load-induced subsidence driven by the presence of the overlying sediments and the water body, and (2) the tectonically driven subsidence. The second curve, the tectonic subsidence, is obtained after subtracting the load-induced component from the total basement subsidence and it reflects solely the tectonic or driving mechanism of a basin (Bond and Kominz, 1984).

A reference model is used for backstripping with a crustal thickness of 36 km and a crustal density of 2.9 g/cm^3 (Table 1).

4.2 Forward models

A model was presented by Van Wees and Beekman (2000) for automatic forward modelling of subsidence data. This approach has been further developed and extended to account for important effects for heat flow and maturity modelling (Van Wees et al., in press).

Both, pure-shear uniform stretching (McKenzie, 1978) as well as depth-dependent differential stretching (e.g. Royden and Keen, 1980) can be simulated with the modelling approach. Furthermore, the effects of underplating can be determined. The thermal evolution is calculated for the syn-rift evolution and subsequent phases of cooling (Van Wees and Stephenson, 1995). Here, a minimisation technique is used to evaluate those stretching parameters that reproduce the 'observed' tectonic subsidence best. Predefined parameters are listed in Table 1 and comprise among others the initial thickness of the crust and lithosphere as well as the onset and duration of rifting (Van Wees and Beekman, 2000 and references therein). A detailed description of the modelling procedure and the physical background is given by Van Wees and Beekmann (2000) and Van Wees et al. (in press).

The uniform stretching model predicts the first-order lithospheric responses to continental extension, notably crustal thinning and geotherm perturbation (McKenzie, 1978; Kusznir et al., 1995). Two competing mechanisms proceed during rifting: lithospheric thinning is associated with an isostatic response of subsidence, whereas the disturbed lithospheric temperature field and the linked increase in the geothermal gradient causes uplift. The perturbed temperature field re-equilibrates in an exponential manner after rifting ceases. The subsidence curves are characterised by rapid subsidence first, followed by increasingly slowing subsidence in the post-rift phase. The respective decay time is about 60-70 Ma (Bott, 1992; Kusznir et al., 1995; Roberts et al., 1998).

Departures from the subsidence predicted by the uniform stretching model can be interpreted as additional thermal disturbances to the basin system that are not accounted for. These thermal disturbances may be a result of multi-phase, differential stretching or of magmatic underplating or a superposition of both (Kusznir et al., 2005, Van Wees et al., in press.). The magmatic character of the South African continental margin and the presence of

a high density, high velocity body in the lower crust indicate that underplating has influenced the margin.

Furthermore, the observed phases of uplift and erosion in the late drift phase as well as the elevated vitrinite reflectance values point to thermal uplift related to phases of mantle attenuation long after continental break up. We therefore evaluated the thermal consequences of these processes for the Orange Basin.

4.3 Heat flow

A forward model which represents the best-fit tectonic model in thus it reproduces the observed present-day sediment geometry includes departures from a classical uniform stretching model. However, the models should also be consistent with the observed vitrinite reflectance profiles. Accordingly, we evaluate the thermal history predicted by the forward model and investigate implications for the hydrocarbon generation. Especially, since the basement heat flow is an influential parameter on the maturity of organic matter throughout basin evolution. The modelling approach enables the calculation of maturation based on probabilistic heat flow scenarios, taking uncertainties from lithospheric thinning into account. Furthermore, the effects of depth-dependent porosities and related changes in thermal conductivity are considered (cf. Van Wees et al., in press). We used the calculated basement heat flow of the best fit tectonic model for the maturation modelling adopting the kinetics of kerogen typ IV and incorporating the activation energies of Burnham and Sweeney (1989).

Uncertainties related to parameters such as lithospheric and crustal thickness, estimates on erosion, paleo water depth and the porosity-depth relations are evaluated in a sensitivity analysis and help to define critical parameters in the modelling approach. These uncertainties can be narrowed if information on temperatures and maturation in the wells is provided. Such data were available for the Orange Basin and have been used to cross-check the forward models thermally.

5 Results

First, we present and discuss different 1D models consistent with the constraints available for the wells. Beside the stratigraphy and lithology-dependent physical properties (Table 1) these constraints include vitrinite reflectance data. Subsequently, the model that reproduces the observed tectonic subsidence and vitrinite reflectance best is applied to synthetic wells created for the gridpoints of the 3D model to derive predictions for un-drilled areas.

5.1 Tectonic subsidence

Figure 7a shows a compilation of the tectonic subsidence curves after backstripping of the wells. All curves are characterised by a moderate slope of initial subsidence as long as the rifting proceeds from 136 until 117.5 Ma. The transition to the drift stage is linked with an increase in subsidence rates from 117.5 to 112 Ma. For most of the wells the gradient is considerably steeper in the early post-rift phase than during initial (syn-rift) subsidence.

Subsequently, from Aptian (112 Ma) until the middle Cenomanian (93 Ma) the steepness of the curves decreases again and they continue in a rather moderate pattern, characteristic for ‘normal’ thermal subsidence. Within the time interval until 85 Ma the margin experiences a phase of tectonic quiescence and displays a rather stable phase of margin evolution.

Around 74 Ma, all the wells are affected by relatively rapid uplift which correlates with the onset of erosion as documented in the wells. The estimated amount of erosion is based on seismic interpretation and consistent with the erosion maps given in Figure 6. Depending on the position of the individual wells and the amount of eroded material, the pure tectonic uplift varies between 126 m for well P-F1 and 75 m for well A-C3.

The time interval from 67 Ma until the onset of the next erosional phase at 16 Ma is not well resolved within the wells and gives no information on how the margin evolved in the meantime. 16 Ma ago, erosion initiated and, linked to that, margin uplift is documented in the tectonic subsidence curves. From 16 to 14 Ma the amount of uplift ranges from 368 m (well A-C2) to 320 m (well A-N1).

From 14 Ma until today the margin is affected by moderate subsidence. No further data points are available from well logs within this interval which renders a better resolved, detailed subsidence reconstruction impossible. Again, the only source of information is seismic data that image a highly variable appearance of this youngest layer where particularly slumping makes a correlation between individual wells difficult.

The reconstruction of a geohistory is prone to uncertainties concerning errors in the used paleo water depths, decompaction parameters, the amount of eroded material and errors in the applied reference model. We found that the investigated variations in these parameters resulted in variance of generally less than 70 m for each data point in the backstripped curves.

5.2 Forward models

5.2.1 McKenzie versus underplating model

After having obtained the tectonic subsidence history for all wells from backstripping, we tried to find forward models that reproduce this 'observed' subsidence pattern. The initial setting for all tested models consists in a lithosphere with an initial thickness of 146 km including a crust 36 km thick. Both numbers are based on literature values and/or were determined in sensitivity tests using the basin history inversion.

The models that fit the observed tectonic subsidence best are plotted for all wells in Figure 7b. The model obtained for well A-C1 is shown to illustrate the differences between the tested forward models and the results are discussed substitutional for all wells in the following. As additional information, basement subsidence as well as tectonic subsidence and paleo water depth are shown for reference (Figure 8).

In the first instance, a uniform stretching model was tested in order to fit the 'observed' tectonic subsidence (Figure 8b, red curve). Due to uniform instantaneous stretching by a factor ß=1.46 for both, the crust and the mantle, an initial basin of 602 m depth is created and the thickness of the present-day crystalline crust is predicted to be 24.6 km. The results

of this forward model give 10 km more in crustal thickness as predicted by the gravity model (Hirsch et al., 2007) which calls for more intensive stretching. An intensification of the stretching would further deepen the initial basin which is already far too deep when compared to the basin depth of 305 m in the backstripped curves.

Thermal cooling commences subsequent to the rifting phase and uniform continuous subsidence creates a basin of steadily increasing depth consistent with present-day basement depth. Neither variation of ß nor of the initial lithosphere thickness reproduced the 'observed' tectonic subsidence as the initial subsidence always was too fast, and, of course, later phases of erosion remain unconsidered in a McKenzie model. Therefore, a number of effects have been included in the forward models which depart from the uniform stretching model.

We evaluated the effect of underplating which is considered to be cumulatively emplaced in the syn-rift phase in our forward models. The density of molten rocks generated by decompressional melting is midway between the density of continental and oceanic crust and ranges between 2990 and 3070 kg/m³ for potential temperatures of 1280°C and 1480°C (Allen and Allen, 2006). Therefore, the density of the underplated material was defined to be 3000 kg/m³ and we assume an emplacement temperature of 1300°C. Lithospheric mantle (density of 3300 kg/m³) is replaced if these melts are trapped underneath the crust and the resulting net-effect when isostasy applies is uplift compared to a uniform stretching model without magmatic activity. Assuming that the lower crustal, high density body modelled for the same study area by Hirsch et al. (2007) represents the present-day relict of the syn-rift underplating we use the configuration of this body as constraint in the forward model (Figure 4a). Accordingly, the respective thickness of the underplated material for well A-C1 is 12 km and it varies between 3 and 14 km across the rest of the working area.

The consideration of the underplated body decreases the slope of the initial subsidence to 165 m in the forward models, and thus results in a better match with the backstripped tectonic subsidence than achieved by the uniform stretching model (Figure 8b, green curve).

Furthermore, the thermal regime of early stages of basin evolution is affected since the addition of hot material increases the heat flow significantly (Allen and Allen, 2006; Fjeldskaar et al., 2003). The respective heat flow evolution is compared for both, the McKenzie and the underplating model in Figure 9. In the uniform stretching case, rifting is accompanied by an increase in basement heat flow of ~10 mW/m². Incorporating underplating elevates the peak heat flow by ~50 mW/m² to ~100 mW/m² for the syn-rift phase.

The forward model obeying the principles of McKenzie predicts a lithospheric thinning of 30% for well A-C1. In contrast, the emplacement of a 12 km thick underplating enforced stronger thinning of the crust to ~10 km (β=3.27) which is consistent with the crustal structure presented by Hirsch et al. (2007). Our approach is based on the assumption that the cumulative emplaced underplated body per se is not affected by stretching. This might represent an oversimplification of the problem but helps to get a first order idea on the effects of underplating. Since mantle material is replaced, the net effect is reduced initial subsidence in the syn-rift phase compared with the uniform stretching model. The underplated body becomes part of the crystalline crust within the post-rift phase. Thus, the cumulative thickness of the crust becomes 22 km and the effective thinning factor 1.64.

Summing up, the model changed due to the presence of the underplating into a depth-dependent stretching model. Underplating not only significantly influences the initial stages of basin evolution, but also affects the post-rift subsidence pattern. Due to the addition of further, hot material the post-rift thermal cooling becomes more effective and the final basement depth is predicted to be much deeper than observed (Figure 8b, green curve).

Though implementing underplating in the early stages of basin evolution improves the fit between observations and forward models, the model does not account for the observed phases of uplift during the late drift phase. These phases are, however, observed and require explanation. Phases of late tectonic uplift are documented for many passive margins and the related mechanisms are still a matter of debate (Fjeldskaar et al., 2003; Gernigon et al., 2004; Watts and Fairhead, 1999). Possible causes behind margin uplift include phases of

sub-crustal thinning, rift shoulder uplift in consequence of renewed extension, far-field compression due to ridge push forces or additional thinning of the sub-crustal mantle in response to either mantle plumes or small-scale convection (Boutillier and Keen, 1999). As neither indication for compressive deformation nor for extensional faulting are present in the seismic data of the Orange Basin, we explore how far the effects of sub-crustal thinning prior to the two major phases of uplift are consistent with the observed tectonic history and thermal maturation data.

5.2.2 Depth-dependent model

Seismic and well data document two phases of erosion that have removed in places up to 500 m of sediments. Thus, the second tested departure from the uniform stretching model was the implementation of mantle thinning coeval to the observed erosional phases to account for thermal uplift. The thinning of the lithospheric mantle provokes upwelling of the asthenosphere. Hence, denser lithospheric mantle is replaced by less dense asthenospheric material and results in isostatic uplift. If the net uplift surpasses the erosional level, material is removed from the system which in turn results in a mass deficit. This prevents complete re-equilibration of the system during post-rift cooling and therefore leads to net subsidence.

The effect of mantle thinning on the forward model is demonstrated for well A-C1 (Figure 9). The lithosphere is thinned to ~85 km in the syn-rift phase. Subsequently, thermal re-equilibration thickens the lithosphere again and at 74 Ma, more than 40 Ma later, the lithosphere almost regained its initial thickness. Incorporating initial uniform stretching and underplating, the model does not depart from the previously described models; differences occur in the post-rift phase.

The onset of the elder phase of erosion (74 Ma) is used herein as the beginning of renewed mantle thinning. This new thinning phase reduces the lithospheric thickness to 121 km which corresponds to a cumulative thinning factor of 1.1. Here, the lithosphere is ~20 km less thick than predicted by the uniform stretching model. Considering that the crust has

not been affected by thinning the net thinning factor for the sub-crustal mantle amounts of 1.13 for well A-C1. For the other wells the cumulative thinning factor for the first uplift phase ranges from 1.03 to 1.06 (Table 2).

Ensuing this phase of mantle thinning, relaxation allows the lithosphere to regain its thickness before renewed thinning reduces the thickness again. The onset of erosion is herein used to mark the timing of the second phase of mantle thinning starting at 16 Ma. Since this second phase of erosion is marked by higher sediment denudation, mantle thinning reaches considerably higher values than during the first phase. For well A-C1, the lithosphere is thinned from 135 km to 111 km; this corresponds to a cumulative beta factor of 1.21. The thinning values vary between 1.13 and 1.34 for the other wells (Table 2). Figure 10 shows a compilation of the lithospheric thickness through time for each well.

These modelled phases of mantle thinning prevent thermal re-equilibration of the system and result in higher heat flows compared to the uniform stretching model even though the thinning itself is only linked to minor heat peaks (Figure 9).

5.2.3 Predictions for the 3D geological model

Assuming that the tectonic history derived for the single wells is also valid for the entire study area, the previously described approach has been applied to synthetic wells to derive predictions for areas where no well control is available. Therefore, the 3D geological model of the basin infill (Hirsch et al., 2007) and is used in this study to establish an equidistant grid of 234 synthetic wells with a spacing of ~10 km for which backstripping and forward modelling has been carried out. The geohistory results derived from the real wells have been applied to these synthetic wells to investigate the subsidence history of the Orange Basin in a wider area constrained by seismic data only. Furthermore, spatial variations of parameters could be addressed and quantified throughout the basin. The temporal resolution is slightly different for the synthetic and the real well since the synthetic wells are based on the 3D geological model.

As mentioned earlier, paleo water depth information is crucial in the geohistory analysis. To derive the required paleo water depth for areas without real well control we used a simple approximation. First, we carried out backstripping for all layers of the 3D geological model assuming an air loaded basin and local isostasy (Scheck and Bayer, 1999).

The restoration reconstructs the topography of the respective horizon at the time of deposition. This paleo topography is correct for air-loaded conditions and does not represent the correct bathymetry. Therefore, this topography was subsequently shifted vertically to comply with the constrained paleo water depth reconstruction for the real wells.

Finally, backstripping has been repeated for the virtual wells to derive the tectonic subsidence taking these paleo water depth and the erosional maps derived from seismic interpretation into account.

The derived backstripped curves of tectonic subsidence indicate that the post-rift subsidence displays a rather uniform, coeval subsidence pattern in north-south direction (Figure 12a). Whereas, along a east-west profile significant differences in tectonic subsidence occur according to increasing stretching factors from the proximal to the distal domain (Figure 12b). Besides the absolute depth range, all curves show a similar pattern as the same tectonic history is assumed for the entire area covered by the 3D model. Accordingly, the same sequence of events is observed in all synthetic wells.

After rifting had ceased at 117.5 Ma the basin underwent a short phase of relative rapid subsidence until 112 Ma. Within these first 5 Ma, the intensity of sagging is increasing with increasing distance to the coast. From 112 Ma onwards, smooth tectonic subsidence curves of moderate gradients indicate that a tranquil phase of subsidence prevailed in the basin. A minor event of short-lived uplift (91.5 Ma) occurred during this period affecting the entire margin before uniform and moderate subsidence continued until 77.5 Ma. At this point in basin evolution a steeper overall gradient of tectonic subsidence indicates renewed subsidence acceleration before a phase of uplift began at 74 Ma and lasted until 67 Ma.

Following this, the margin experienced renewed, continuous thermal subsidence until 16 Ma. Unfortunately, sparse data coverage prevents further analysis of this time interval.

Thereafter, a second uplift event, larger in magnitude than the previous uplift, affected the basin from 16-14 Ma. Finally, the margin experienced another 14 Ma of subsidence until present-day.

Like in the 1D case for the real wells, the forward models for the synthetic wells predict the tectonic subsidence, the variation of thinning factors for the crust and lithospheric mantle and the thermal history, thus allowing an assessment of these parameters for the entire 2.5D model area.

rifting

The combined effect of uniform stretching and underplating for the initial rifting and the opening of the Orange Basin result in an increasing tectonic subsidence from the proximal to the distal domains of the basin. Accordingly, the tectonic subsidence for this time interval is consistent with the results of backstripping. Tectonic subsidence ranges between no vertical motion near the present coast and increases to 500 m of subsidence in the most distal parts. The effect of underplating prevents subsidence in domains where the effective thinning factor was smaller than 1.6 as the thermal uplift caused by the underplating counteracts the rift induced subsidence. In these domains the margin appears to be unaffected by rifting in terms of initial subsidence. The effective crustal thinning values (beta) vary between 1.0 close to the coast and 2.2 in the distal parts of the model (Figure 13).

At the same time, the lithosphere experiences a thinning to less than 60 km in the distal domains of the model, a thinning to 110 km in the vicinity of the A-wells, and remained un-stretched in the most proximal domains. On the outer margin, where the beta values reach their maximum, the crust was thinned to less than 10 km post-rift thickness, which corresponds to the thickness of the crystalline crust modelled by Hirsch et al. (2007). This already indicates that subsequent phases of tectonics did not lead to any further thinning of the crust, but were related to sub-crustal thinning.

Subsequent to rifting and the emplacement of underplating, thermal cooling started and caused a re-equilibration of the system during which the thickness of the previously stretched

lithospheric mantle was increasing again. This cooling appears to be the dominant driving mechanism for the subsidence of the basin. Accordingly, a deepening of the basin is predicted during the time interval (117.5-112 Ma) with a tectonically induced component of up to maximal 1000 m of subsidence (Figure 14a).

Again, the intensity of tectonic subsidence varies across the margin: On the inner shelf almost no subsidence was active but with increasing distance to the coast the intensity of tectonic subsidence increased and accounted for ~350 m depth near the A-C wells and 1000 m in the outer most domains.

112-93 Ma

From 112 until 93 Ma, the tectonic subsidence declines with respect to the time interval since rifting and varies from 200 m to 700 m across the basin. Maximum tectonic subsidence is focussed in a N-S striking corridor from 112-93 Ma (Figure 14b). The total accumulation space created by tectonics since the onset of rifting results from the superposition of the different phases of tectonic subsidence. Accordingly, the pattern of basement subsidence outlines a NW-SE striking depocentre on the inner margin where most of the sediments were deposited (cf. Figure 3b). Vast amounts of sediments were transported into this paleo depression and built up a delta of up to 1953 m in thickness, whereas the outer margin received only little sedimentation.

Contour lines of predicted temperatures in the Hauterivian potential source rock interval correlate spatially with contour lines of the maximum in sediment accumulation. Calculated paleo temperatures within this source rock interval overstep 100°C in areas where more than 1000 m of sediments accumulated and exhibit a NW-SE striking maximum of up to 170°C where the overlying sediment package attains the largest thickness. In the overlying Barremian/Aptian source rock interval temperatures still exceed 70°C with a maximum of 140°C in the same area.

Thus, the process of sediment deposition dominates the thermal evolution in the sediments rather than the tectonically caused lateral variations in basement heat flow.

93-74 Ma

The tectonic subsidence during the next-younger phase (93-74 Ma) reflects ongoing declining thermal subsidence that varies between ~200 m close to the coast and more than 400 m seawards (Figure 14c). At the end of this time interval at 74 Ma, a preliminary maximum in burial is reached, immediately before the margin experiences a phase of intermediate uplift.

At this stage, not only the basement depth reached a first maximum but also the temperatures within the source rock intervals. The Hauterivian source rock is subjected to 240°C in maximum in the north-western edge of the model. In the vicinity of the A-wells, where the thickest sediment portions were deposited, temperatures range between 140 and 180°C for this source rock. In the shallower Barremian/Aptian source rock interval modelled temperatures range between 120 and 160°C around the A-wells (Figure 15) and the uppermost source rock interval of Cenomanian/Turonian age is subjected to temperatures exceeding 100-140°C.

uplift from 74 - 67 Ma

The next time step in basin evolution from 74 Ma to 67 Ma is characterised by a phase of erosion of the inner shelf area. In order to remove the sediments, the margin must not subside any further but needs to experience uplift to expose sediments to erosion. As detailed for the 1D case, we assume mantle thinning as a possible causative mechanism behind this phenomenon, whereas the thickness of the crust does not experience further changes. So as to reproduce the backstripped tectonic subsidence and the erosion estimates the required thinning of the lithospheric mantle varies between 1.1 and 1.2 (Figure 16a). The pre-uplift thickness of the re-equilibrated lithosphere in consequence of thermal cooling ranges between 120 km in the distal areas of the model and 146 km on the shelf as predicted by the forward model. In consequence of renewed mantle thinning this thickness is reduced to 107-140 km (Figure 16b).

The resulting net effect in terms of vertical, pure tectonically induced movement is a N-S striking corridor, encompassing the A-wells, that is exposed to maximum tectonic uplift of up to 340 m (Figure 17a). Adjacent to this corridor, the uplift exceeds 150 m all over the working area. Accordingly, the basement heat flow evolution from 74 to 67 Ma is characterised by an increase of up to 5 mW/m² on the inner margin (Figure 17b). Spatially, the distribution of the heat flow increase correlates with the area affected by erosion.

67-16 Ma

The deposition of a horizon dated to 67 Ma (22at1) documents the end of erosion and the onset of renewed margin subsidence. The following time interval until 16 Ma is limited upwards by a second major erosional unconformity, but is sparsely documented in the sediment columns since erosion and/or minor accumulation prevented the preservation of thick strata. Sediments are preserved predominantly seaward of the present-day shelf break on the outer margin. According to seismic data, up to 1500 m of sediments are preserved today on the outer margin documenting a rather moderate creation of accommodation space there (Figure 5e). On the inner and middle margin the reconstruction of the second phase of erosion documents the removal of about 500 m of sediments (Figure 6).

Prior to erosion, subsidence proceeded coeval to deposition and re-deepened the basin again until 16 Ma. Between 67 and 16 Ma tectonic subsidence contributed to this process ~300 m on the outer margin, ~450 m in a N-S corridor on the middle margin and less than 350 m farther landward (Figure 14d).

It was during this time interval that the source rocks experienced the deepest burial in the basin history which makes this interval the most interesting interval for hydrocarbon aspects.

Indeed, the model predicts that the temperatures within the source rock intervals exceed the temperatures experienced at 74 Ma as they are now overlain by a thicker sediment cover. In the Hauterivian source rock interval, the sediments of the outer margin are subjected to ~200°C, the middle margin experiences ~150°C, and on the inner margin of ~70°C occur. At a shallower level, the temperatures of the Barremian/Aptian source rocks

still reach ~180°C seaward of the A-wells where the largest sediment thicknesses accumulated. Temperatures decrease to ~120°C farther landward and vary between 70 and 90°C close to the coast (Figure 18). In the Cenomanian source rock interval, temperatures of 150°C are reached in maximum in the distal domains of the model. Temperatures are continuously decreasing to ~90°C farther landward and on the inner margin this interval still has a temperature of ~60°C.

uplift from 16-14Ma

As mentioned above, seismic data document erosion in the late Early Tertiary prior to 14 Ma which was estimated to amount 500 m at maximum (Figure 6b). Again, sub-crustal thinning was modelled to account for uplift and like in the 1D case, a duration of 2 Ma was assumed for the erosion event. The intensity of erosion during this phase of uplift is larger than the intensity of the first erosional phase and accordingly the amount of mantle thinning also exceeds that of the previous thinning event.

For the time interval from 16 to 14 Ma thinning factors for the lithospheric mantle were found to be smaller than 1.2 for the proximal half of the model. In the distal half of the models the factors are round about 1.25 and the thinning factor even overstepped 1.5 in the domain where most of the sediments accumulated (Figure 19).

The lithospheric mantle is thinned according to the distribution of the thinning factors and the stretched thickness varies between 100 km and 130 km.

Tectonic uplift ranged from 150 m to more than 300 m for the first tectonic uplift event (74-67 Ma). The second more effective erosional event is, in turn, linked to more intensive tectonic uplift. The uplift varied between moderate values of 240 m on the outer margin and maximum values of 540 m concentrated on the middle margin, whereas the inner margin experiences 350-400 m of tectonic uplift (Figure 20a).

The increase in basement heat flow from 14 to 16 Ma is less than 8 mW/m² throughout the working area (Figure 20b) and outlines the realm which has been affected by erosion (Figure 6b).

5.2.4 implications for hydrocarbon generation

The forward models described beforehand are used to calculate the temperature history which the single wells experienced. The forward model predicts for well A-C1 a present-day basement heat flow of 51 mW/m² (Figure 9) and accordingly a surface heat flow of about 56 mW/m². These numbers are slightly higher as predicted for old oceanic domains (~50 mW/m²; Stein and Stein, 1992).

The well is underlain by underplating of 12 km. The heat contribution of this mafic feature is negligible at present-day. Since the sediments contribute a maximum of 5 mW/m², the main component of heat flow must originate from the crust and also the mantle.

As a general trend, the vitrinite reflectance measured in the wells of the Orange Basin show elevated values in comparison to the trend in a global compilation and are generally higher than expected from the present-day burial depth (Allen and Allen, 2006 and references therein). This points to a thermal overprint either due to larger initial maximum burial and subsequent erosion or to an additional heating event.

That the calculated values of the vitrinite reflectance according to the best-fit tectonic model do reproduce the measured values in a satisfiable manner (Figure 11a) implies the reliability of the predicted heat flow history to explain the present-day maturity of the sediments. For the A-wells, however, the modelled trend in the vitrinite values is still lower than in the measured samples. Especially in the uppermost 2.5 km, the modelled values are displaced parallel to the measured values. This indicates that sources of error are probably not related to the chosen rock specific parameters as the thermal conductivity or the porosity-depth-relations. Suspicious thermal parameters would rather be expressed in a differing gradient of the vitrinite increase with depth than in a parallel displacement and increased surface values. Therefore, other processes must be responsible for the general misfit. The character of the parallel displacement indicates that a rather young process was active since samples over the entire depth have been affected and overprinted. In a sensitivity analysis,

we evaluated the influence of increased erosion for the second erosional event. If thicknesses, missing due to erosion, are underestimated, also the maximum burial depth and the related maturation of the sediments are underestimated. The amount of eroded material was derived from seismic interpretation which is of course prone to uncertainties. Increasing the amount of erosion for the A-C wells to 1000 m and 900 m respectively results in a good fit between modelled and observed vitrinite reflectance (Figure 11b). This increased erosion/uplift, however, would require further mantle thinning. In detail, this would imply a thinning of the lithosphere to 100 km for well A-C1 for which so far a thickness of 111 km was predicted.

After having cross-checked the thermal predictions of the forward models with existing data it is possible to evaluate the thermal history within the entire working area based on the synthetic wells. The most interesting stages of basin development for hydrocarbon generation are those when the potential source rock intervals experienced maximum temperatures. The maximum temperatures can have been reached in response to maximum burial, due to a thermal overprint, or due to a superposition of both processes. The reconstructed subsidence of the basin documents a phase when the burial depth of the horizons exceeded the depth in which the horizons are found today (c.f. Figure 8a). This maximum burial depth was achieved before the second uplift event 16 Ma ago. Accordingly, this time step is linked to peak temperatures to which the sediments have been subjected to.

The temperatures of the source rock intervals have been reported according to each time step before (cf. Figure 15, Figure 18). The entire temperature evolution is shown for one representative synthetic well in the vicinity of well A-C1 (Figure 21).

Phases of steep gradients in subsidence are also characterised by a steep increase in temperature, such as for the time interval between 117.5 and 103 Ma.

An erosional hiatus between 93.5 and 91.5 Ma is expressed as a minor temperature decrease. Subsequently, steadily proceeding subsidence acts in concert with increasing temperatures which reach a preliminary maximum at 74 Ma, before a temperature decrease documents the uplift the margin is subjected to. The maximum temperatures of 165°C are

reached when the sediments experienced maximum burial at 16 Ma. The Hauterivian and the Barremian/Aptian source rock interval enter the maturity window of oil and gas generation when overstepping 0.5 in vitrinite reflectance at 95.5 and 93 Ma, respectively (Figure 22).

The cracking of oil to gas commences at a vitrinite reflectance value of 0.8 which starts for the deepest source rock at 85 Ma and for the Barremian/Aptian one around 77.5 Ma. Both exceed 1.0 in vitrinite reflectance at 77.5 and 67 Ma. The latter boundary is not exceeded by the youngest and most speculative source rock interval of Cenomanian/Turonian age, which remained in the oil and gas generation window from 85 Ma until 16 Ma. In contrast to the temperature evolution, short phases of tectonic activity are not expressed in the maturity evolution.

In response to the repeated shifts of depocentres the appraisal of present-day prospectivity should consider the spatial variation of the maturity related to the different source rocks at the time of deepest burial (16 Ma). At this time, the Hauterivian source rock is predicted to have a maturity of more than 1.2 all across the outer margin and even more than 2.2 in the domains of largest sediment accumulation (Figure 23a). The same area is also more mature than 1.5 in the overlying Barremian/Aptian source rock interval, which reaches values of about ~1.0 on the outer margin (Figure 23b). The Cenomanian/Turonian source rock reaches ~0.6 on the middle margin which increases farther seaward to ~0.7 and to more than 1.0 in the domain of largest sediment thicknesses (Figure 23c).

6 Discussion and Conclusions

Our attempt to reconstruct the subsidence history in the Orange Basin revealed that a simple uniform stretching model is insufficient to explain the observed subsidence history in that it does neither predict the observed slope of initial tectonic subsidence nor Cenozoic phases of uplift. Only depth-dependent lithospheric thinning with thinning of the sub-crustal

mantle can account for the subsidence history and the thermal evolution consistent with seismic data and measured vitrinite reflectance.

The forward models which reproduce the observed subsidence history best include two departures from the uniform stretching model: First, underplating has been implemented considering the geometry of a high velocity, high density lower crustal body according to the study of Hirsch et al. (2007). The presence of these lower crustal bodies is a common feature along many volcanic passive continental margins (Watts and Fairhead, 1999) and for the study area, not only suggested by gravity modelling (Hirsch et al., 2007), but also proven by seismic refraction data (Hirsch et al., in press). In spite of a still ongoing discussion, these lower crustal bodies are interpreted as a result of magmatic underplating. Accordingly, this underplated material represents both ponded magmatic material trapped beneath the Moho and magmatic sills injected into the lower crust (Cox, 1992; Rutter et al., 1993; Thybo et al., 2000; White and McKenzie, 1989).

Observations supporting underplating occurring coevally with initial rifting include surface uplift, massive sand influx and the low subsidence rate during and after the break up (Maclennan and Lovell, 2002). The production of the required melts is still a matter of debate and may be a result of elevated potential temperature of the mantle, of high extension rates, of small-scale convection, or of fertile patches in the upper mantle (Boutillier and Keen, 1999; Buck, 1991; Foulger and Anderson, 2005; Korenaga, 2004; McKenzie and Bickle, 1988; Nielsen and Hopper, 2002; Pedersen and van der Beek, 1994; Van Wijk et al., 2001; Wilson, 1993). It is beyond the scope of this study to discriminate between causative mechanisms. Instead we aimed to assess the consequences of underplating for the subsidence and heat flow history. Our results confirm earlier studies (Fjeldskaar et al., 2003; Gernigon et al., 2004) in that the main effects of underplating in comparison to the uniform stretching model are the reduction of the initial subsidence, the significant but short termed increase in heat flow, and the enhanced post-rift subsidence due to the addition of further, hot material.

A second departure from the uniform stretching model is needed, since from initial rifting with coeval underplating alone, a much deeper basin is predicted than observed today and

phases of intervening uplift in the Cenozoic would remain unexplained. This second departure consists of renewed sub-crustal thinning at times for which erosion is observed. A reactivated rifting of the sub-crustal domain interrupts the thermal subsidence in consequence of the initial rifting and induces uplift which is consistent with erosional unconformities documented in the seismic data and in the wells. In addition, sub-crustal thinning creates elevated heat flow scenarios. These scenarios seem to be appropriate since the thermal maturity of sediments within the Orange Basin shows higher values than would correspond to their present burial depth or any uniform stretching model. In parts (A-C wells), even more erosion than suggested by seismic interpretation and, linked to that, mantle thinning is required to reproduce the observed maturity of the sediments.

The Cenozoic phases of uplift are more difficult to explain dynamically. Again, the phenomenon of post-break up phases of uplift is observed at many passive margins but proposed mechanisms are the topic of controversy (Jackson et al., 2005). Post-break up margin uplift may be a consequence of a rising mantle superswell (Burke, 1996; Gurnis et al., 2000; Nyblade and Robinson, 1994), of residual effects of long-lived Mesozoic plume heads and tails (Nyblade and Sleep, 2003), of lithospheric folding and thermal softening in response to ridge-push forces (Ayele, 2002), of small-scale convection (Huismans and Beaumont, 2008), or even of a renewed pulse of lithospheric extension in response to a change in plate rotation poles (Guiraud and Bosworth, 1997; Nürnberg and Müller, 1991). For passive margins west and south of South Africa a temporal correlation is reported between phases of margin uplift, phases of increased denudation of the continent onshore (Kounov et al., 2007) and phases of Kimberlite emplacement (de Wit, 2007; Tinker et al., 2008), that points to processes affecting the lithospheric and sub-lithospheric mantle.

Rift shoulder uplift might provide a mechanism to explain the observed onshore topography including the Great Escarpment even though its origin and age is subjected to a controversy. Linked to that, flexural uplift due to isostatic rebound in response to erosion of the rift shoulders, can extend far into the basin and can cause uplift of the shelf (Burov and

Cloetingh, 1997; Van Balen et al., 1995) but would not explain the phases of renewed subsidence subsequent to uplift.

The presence of the Great Escarpment might argue for a hybrid rifting model of simple shear in the upper crust on listrict or planar faults whereas the pure shear occurs in the ductile lower crust and mantle lithosphere (Kusznir et al., 1991). Seismic data do not indicate the presence of listric or planar faults cutting through the crust or upper mantle which discards this theory for explanation.

Another outcome of this study is the present-day heat flow in the basin. The values, as shown for well A-C1, are slightly higher than predicted for an old oceanic domain but in good agreement with heat flow values predicted by Goutorbe et al. (2008). Consistent with their results we found the contribution of the sediments to the surface heat flow to be less than ~5 mW/m². Since the contribution of the underplated body to the heat flow is negligible, the main component of the 50-60 mW/m² must be contributed by the crust and the mantle. Following their argumentation, there is a stark contrast between the estimated heat flow values of 17-30 mW/m² for the onshore Archean craton and the Proterozoic belts. The modelling results show an increase in surface heat flow across the margin with the highest values distal to the coast. Thus, the radiogenic heat production of the crust is inapplicable to explain the increase since the crust thins towards the ocean (Goutorbe et al., 2008). Global heat flow maps inferred from global seismic models show that continental margins are characterised by higher heat flow values as the adjacent oceanic and continental domains (Shapiro and Ritzwoller, 2004). This modelling is consistent with findings presented by Lucazeau et al. (2004) who found a similar heat flow distribution across the margin offshore Angola with the highest values on the continental shelf. They argue for an edge effect caused by an abrupt change in lithospheric thickness inducing convective patterns at the base of the lithosphere. Such an increase in heat flow over a relatively short distance could be reproduced in laboratory experiments (Guillou and Jaupart, 1995).

The lack of extensive volcanism within South Africa (Burke, 1996) today seems to rule out a thermal anomaly directly within or beneath the lithosphere. Several studies suggested that

discontinuities in lithospheric thickness may result in small-scale convective instabilities which might cause surface topography anomalies and/ or tectonic features. Small-scale convection models have been proposed with a downwelling that remains fixed at the margin of the craton whilst the upwelling moves off the spreading axes of the ocean basin (King and Ritsema, 2000). The downwelling would cause a cold thermal anomaly and could therefore account for lithospheric thinning in the absence of a positive anomaly.

The absence of volcanism in combination with the observed seismic structure of the lithosphere does not support models which suggest the emplacement of a Cenozoic mantle plume even if such a plume could account for the present-day elevation of south Africa. Even two starting mantle plume heads, one at the time of Karoo volcanism (ca. 183 Ma) and the other at the time of Kimberlite eruption (ca. 80–90 Ma) cannot produce much (< 200 m) of the present-day anomalous elevation (Nyblade and Sleep, 2003). Only if the plume tails linger beneath the lithosphere for ~25–30 Ma, ~500 m of present-day elevation could be reproduced but this theory also fails to explain the phases of uplift and subsidence by turns.

It has been found that the velocity of the deep mantle underneath South Africa is lower than average which is typical for hot regions (Gurnis et al., 2000). The interpretation of this anomaly is that it represents a long-lived hot mantle upwelling which correlates spatially with long-wavelength geoid highs (Gurnis et al., 2000). Africa has the highest elevation of a continent probably indicative of uplift supported by very deep seated flow in the lower mantle.

A state of horizontal compression is proposed for the Lower Congo Basin from the analysis of fault mechanisms for 5 earthquakes controlled by distant plate-boundary forces (Ayele, 2002). Compression would thus support the existence of lithospheric folding (e.g. Cloetingh and Burov, 1996; Cloetingh et al., 1999) as a candidate to explain the observed uplift. This compression could be induced by ridge-push of the Mid-Atlantic Ridge on the western plate boundary acting in concert with extension in the East African Rift System at the eastern plate boundary. On the other hand, the spreading rates between South America and Africa have been continuously decreasing since the onset of drifting (Müller et al., 1997). Therefore, it is questionable whether distant plate-boundary forces are causative mechanisms for the uplift

observed in the South Atlantic. Furthermore, no compressional features are observed in our study area which is used as an argument to reject lithospheric buckling as causative mechanism.

Our results confirm the necessity to involve sub-crustal thinning in order to explain the observed post-break up subsidence and the maturation of organic matter. If this mantle thinning is a consequence of any of the mantle processes presently discussed can not be deduced from our analysis but would require additional deep seismic and seismologic investigations.

In summary, our model predicts a syn-break up setting characterised by shallow water depth and high heat flow due to differential thinning and associated underplating, subjected to subsequent thermal cooling and affected by two additional phases of sub-crustal thinning about 70 Ma after break up. This concept is not only supported by the preserved sediment record and the evolution of tectonic subsidence but also by the crustal configuration observed today (Bauer et al., 2000; Hirsch et al. 2007, in press). Finally, the modelled thermal history suggests that the potential source rocks may have generated petroleum in the past and, provided adequate reservoir rocks and an intact seal exist, prospective petroleum systems may be present in the area.

Acknowledgements

This work has been done in the framework of INKABA yeAFRICA at the Helmholtz – Zentrum Potsdam Deutsches GeoForschungsZentrum-GFZ.

Isostatic modelling was performed with the Geological Modelling System (GMS) developed at Helmholtz–Zentrum Potsdam Deutsches GeoForschungsZentrum-GFZ, Department Organic Geochemistry under the leadership of Prof. Dr. U. Bayer.

Many thanks go to Bruno Goutorbe for providing temperature data. Heinz-Gerd Holl is thanked for discussing the porosity logs and Ian McMillan for help with the paleo water depths.

Maps were plotted using GMT 4.0 (http://gmt.soest.hawaii.edu/).

We want to thank cordially Marie-François Brunet and an anonymous reviewer for their constructive comments which helped to improve the quality of the manuscript decisively.

References

Airy, G.B., 1855. On the Computation of the Effect of the Attraction of Mountain-Masses, as Disturbing the Apparent Astronomical Latitude of Stations in Geodetic Surveys. Philosophical Transactions of the Royal Society of London, 145, 101-104.

Allen, P.A. and Allen, J.R., 2006. Basin Analysis: principles and applications. Blackwell Science Ltd., Oxford, 549 pp.

Ayele, A., 2002. Active compressional tectonics in central Africa and implications for plate tectonic models; evidence from fault mechanism studies of the 1998 earthquakes in the Congo Basin. Journal of African Earth Sciences, 35(1), 45-50.

Bauer, K., Neben, S., Schreckenberger, B., Emmermann, R., Hinz, K., Fechner, N., Gohl, K., Schulze, A., Trumbull, R. B., and Weber, K., 2000. Deep structure of the Namibia continental margin as derived from integrated geophysical studies. Journal of Geophysical Research, 105(B11), 25,829-25,853.

Bond, G.C. and Kominz, M.A., 1984. Construction of tectonic subsidence curves for the early Paleozoic miogeocline, southern Canadian Rocky Mountains; implications for subsidence mechanisms, age of breakup, and crustal thinning. Geological Society of America Bulletin, 95(2): 155-173.

Bott, M.H.P., 1992. Passive margins and their subsidence. Journal of the Geological Society, 149(5), 805-812.

Boutilier, R.R. and Keen, C.E., 1999. Small-scale convection and divergent plate boundaries. Journal of Geophysical Research, 104(B4), 7389-7403.

Broad, D.S., Jungslager, E.H.A., McLachlan, I.R., Roux, J., 2006. Offshore Mesozoic Basins. In: M.R. Johnson, Anhaeusser, C.R., Thomas, R.J. (Editor), The Geology of South Africa. Geological Society of South Africa, Johannesburg/Council for Geosciences, Pretoria, pp. 553-571.

Brown, L.F., Jr., Benson, J.M., Brink, G.J., Doherty, S., Jollands, A., Jungslager, E.H.A., Keenan, J.H.G., Muntingh, A., and van Wyk, N.J.S., 1995. Sequence stratigraphy in offshore South African divergent basins: an atlas on exploration for Cretaceous

lowstand traps by SOEKOR (Pty) Ltd. American Association of Petroleum Geologists, Studies in Geology, 41, 184 pp.

Buck, W.R., 1991. Modes of continental lithospheric extension. Journal of Geophysical Research, 96(B12), 20,161-20,178.

Burke, K., 1996. The African Plate. South African Journal of Geology, 99(4), 339-409.

Burnham, A.K. and Sweeney, J.J., 1989. A chemical kinetic model of vitrinite maturation and reflectance. Geochimica et Cosmochimica Acta, 53(10), 2649-2657.

Burov, E. and Cloetingh, S., 1997. Erosion and rift dynamics; new thermomechanical aspects of post-rift evolution of extensional basins. Earth and Planetary Science Letters, 150(1-2), 7-26.

Cloetingh, S., Burov, E. and Poliakov, A., 1999. Lithosphere folding; primary response to compression? (from Central Asia to Paris Basin). Tectonics, 18(6), 1064-1083.

Cloetingh, S. and Burov, E.B., 1996. Thermomechanical structure of European continental lithosphere; constraints from rheological profiles and EET estimates. Geophysical Journal International, 124(3), 695-723.

Corcoran, D.V. and Clayton, G., 2001. Interpretation of vitrinite reflectance profiles in sedimentary basins, onshore and offshore Ireland. In: P.M. Shannon, P.D.W. Haughton and D.V. Corcoran (Editors), The petroleum exploration of Ireland's offshore basins. Geological Society Special Publications, pp. 61-90.

Cox, K.G., 1992. Karoo igneous activity, and the early stages of the break-up of Gondwanaland. Geological Society Special Publications, 68, 137-148.

de Wit, M.J., 2007. The Kalahari Epeirogeny and climate change; differentiating cause and effect from core to space. South African Journal of Geology, 110(2-3), 367-392.

de Wit, M., J. Stankiewicz, J. Restoring, 15.-20. April 2007. Pan African-Brasiliano connections: more Gondwana control, less Trans-Atlantic corruption, EGU 2007-A-06500, Vienna, Austria.

Dow, W.G., 1977. Kerogen studies and geological interpretations. Journal of Geochemical Exploration, 7, 79-99.

Eglington, B.M. and Armstrong, R.A., 2003. Geochronological and isotopic constraints on the Mesoproterozoic Namaqua-Natal Belt; evidence from deep borehole intersections in South Africa. Precambrian Research, 125(3-4): 179-189.

Faulkner, P.A., 2000. Tectonic and thermal evolution of South Atlantic marginal basins, University of Cambridge.

Fjeldskaar, W., Johansen, H., Dodd, T.A. and Thompson, M., 2003. Temperature and maturity effects of magmatic underplating in the Gjallar Ridge, Norwegian Sea, Multidimensional basin modeling. American Association of Petroleum Geologists (AAPG/Datapages), Tulsa, OK, United States, pp. 71-85.

Foulger, G.R. and Anderson, D.L., 2005. A cool model for the Iceland hotspot. Journal of Volcanology and Geothermal Research, 141(1-2), 1-22.

Gernigon, L., Ringenbach, J.-C., Planke, S. and Le Gall, B., 2004. Deep structures and breakup along volcanic rifted margins: insights from integrated studies along the outer Voring Basin (Norway). Marine and Petroleum Geology, 21(3), 363-372.

Gerrard, I. and Smith, G.C., 1982. Post-Paleozoic succession and structure of the southwestern African continental margin. In: J.S. Watkins, Drake, C.L. (Editor), Studies in Continental Margin Geology. American Association of Petroleum Geologists Memoir, Tulsa, pp. 49-74.

Gladczenko, T.P., Hinz, K.,Eldholm, O., Meyer, H., Neben, S., Skogseid, J., 1997. South Atlantic volcanic margins. Journal of the Geological Society, 154(3), 465-470.

Gladczenko, T.P., Skogseid, J. and Eldholm, O., 1998. Namibia volcanic margin. Marine Geophysical Researches, 20(4), 313-341.

Goutorbe, B., Lucazeau, F. and Bonneville, A., 2008. The thermal regime of South African continental margins. Earth and Planetary Science Letters, 267(1-2), 256-265.

Grunow, A., Hanson, R., and Wilson, T., 1996. Were aspects of Pan-African deformation linked to Iapetus opening? Geology, 24(12): 1063-1066.

Guillou, L. and Jaupart, C., 1995. On the effect of continents on mantle convection. Journal of Geophysical Research, 100(B12), 24,217-24,238.

Guiraud, R. and Bosworth, W., 1997. Senonian basin inversion and rejuvenation of rifting in Africa and Arabia; synthesis and implications to plate-scale tectonics. Tectonophysics, 282(1-4), 39-82.

Gurnis, M., Mitrovica, J.X., Ritsema, J. and van Heijst, H.-J., 2000. Constraining mantle density structure using geological evidence of surface uplift rates, The case of the African Superplume. Geochemistry, Geophysics, Geosystems - G (super 3), 1(7), Paper Number 1999GC000035.

Hälbich, I.W. (1993). Cape Fold Belt- Agulhas Bank Transect across Gondwana suture, southern Africa. American Geophysical Union Special Publication, 202, 18pp and maps.

Haq, B.U., Hardenbol, J. and Vail, P.R., 1988. Mesozoic and Cenozoic chronostratigraphy and cycles of sea-level change. In: C.K. Wilgus, Ross, C.A., Posamentier, H. (Editor), Sea Level change: an integrated Approach. Special Publication - Society of Economic Paleontologists and Mineralogists, pp. 72-108.

Herbin, J.P., Muller, C., de Graciansky, P. C., Jacquin, T., Magniez-Jannin, F., Unternehr, P., Dias-Brito, Dimas, 1987. Cretaceous anoxic events in the South Atlantic. Revista Brasileira de Geociencias, 17(2), 92-99.

Héroux, Y.A., Chagnon, A. and Bertrand, R., 1979. Compilation and correlation of major thermal maturation indicators. AAPG Bulletin, 63, 2128-2144.

Hinz, K., 1981. Hypothesis on terrestrial catastrophes: wedges of very thick oceanward dipping layers beneath passive continental margins - their origins and paleoenvironmental significance. Geologisches Jahrbuch, Series E, 22, 1-28.

Hirsch, K.K., Bauer, K. and Scheck-Wenderoth, M., 2008. Deep structure of the western South African passive margin - Results from a combined approach of seismic, gravity and isostatic investigations. Tectonophysics.

Hirsch, K.K., Scheck-Wenderoth, M., Paton, D.A. and Bauer, K., 2007. Crustal structure beneath the Orange Basin, South Africa South African Journal of Geology, 110(2/3), 249-260.

Huismans, R.S. and Beaumont, C., 2008. Complex rifted continental margins explained by dynamical models of depth-dependent lithospheric extension. Geology (Boulder), 36(2), 163-166.

Jackson, M.P.A., Hudec, M.R. and Hegarty, K.A., 2005. The great West African Tertiary coastal uplift; fact or fiction? A perspective from the Angolan divergent margin. Tectonics, 24(6), 23.

Jungslager, E.H.A., 1999. Petroleum habitats of the Atlantic margin of South Africa. In: N.R. Cameron, Bate, R. H. & Clure, V. S. (Editor), The Oil and Gas Habitats of the South Atlantic. Geological Society Special Publication, London, pp. 153-168.

King, S.D. and Ritsema, J., 2000. African hot spot volcanism; small-scale convection in the upper mantle beneath cratons. Science, 290(5494), 1137-1140.

Korenaga, J., 2004. Mantle mixing and continental breakup magmatism. Earth and Planetary Science Letters, 218(3-4), 463-473.

Kounov, A., Niedermann, S., de Wit, M. J., Viola, G., Andreoli, M., Erzinger, J., 2007. Present denudation rates at selected sections of the South African escarpment and the elevated continental interior based on cosmogenic (super 3) He and (super 21) Ne. South African Journal of Geology, 110(2-3), 235-248.

Kuhlmann, G., R. di Primio, D. van der Spuy and Horsfield, B., 2008. Implications of Slope Failures for the Hydrocarbon System in the Orange Basin, Offshore South Africa, AAPG Annual Convention and Exhibition, San Antonio, Texas.

Kusznir, N.J., Hunsdale, R., Roberts, A.M. and iSIMMTeam, 2005. Timing and magnitude of depth-dependent lithosphere stretching on the southern Lofoten and northern Vøring continental margins offshore mid-Norway: implications for subsidence and hydrocarbon maturation at volcanic rifted margins. In: A.G.V. Doré, B. A. (Editor), Petroleum Geology: North-West Europe and Global Perspectives—Proceedings of the 6th Petroleum Geology Conference. Petroleum Geology Conferences Ltd. Published by the Geological Society, London, pp. 767-783.

Kusznir, N.J., Marsden, G. and Egan, S.S., 1991. A flexural-cantilever simple-shear/pure-shear model of continental lithosphere extension; applications to the Jeanne d'Arc Basin, Grand Banks and Viking Graben, North Sea. Geological Society Special Publications, 56, 41-60.

Kusznir, N.J., Roberts, A.M. and Morley, C.K., 1995. Forward and reverse modelling of rift basin formation. In: J.J. Lambiase (Editor), Hydrocarbon Habitat in Rift Basins. Geological Society, London, pp. 33-56.

Lucazeau, F., Brigaud, F. and Bouroullec, J.L., 2004. High-resolution heat flow density in the Lower Congo Basin. Geochemistry, Geophysics, Geosystems - G (super 3), 5, doi:10.1029/2003GC000644.

Maclennan, J. and Lovell, B., 2002. Control of regional sea level by surface uplift and subsidence caused by magmatic underplating of Earth's crust. Geology (Boulder), 30(8), 675-678.

McKenzie, D., 1978. Some remarks on the development of sedimentary basins. Earth and Planetary Science Letters, 40(1): 25-32.

McKenzie, D. and Bickle, M.J., 1988. The volume and composition of melt generated by extension of the lithosphere. Journal of Petrology, 29(3), 625-679.

McMillan, I.K., 2003. Foraminiferally defined biostratigraphic episodes and sedimentation pattern of the Cretaceous drift succession (Early Barremian to Late Maastrichtian) in seven basins on the South African and southern Namibian continental margin. South African Journal of Science, 99(11-12), 537-576.

Müller, R.D., Roest, W.R., Royer, J.-Y., Gahagan, L.M. and Sclater, J.G., 1997. Digital isochrons of the world's ocean floor. Journal of Geophysical Research, 102(B2), 3211-3214.

Muntingh, A. and Brown, L.F.J., 1993. Sequence stratigraphy of the petroleum plays, postrift Cretaceous rocks (lower Aptian to upper Maastrichtian), Orange Basin, western offshore, South Africa. In: P. Weimer, Posamentier, H.W. (Editor), Siliclastic

Sequence Stratigraphy - recent developments and applications. American Association of Petroleum Geologists Memoir, Tulsa, pp. 71-97.

Nielsen, T.K. and Hopper, J.R., 2002. Formation of volcanic rifted margins; are temperature anomalies required? Geophysical Research Letters, 29(21), 4.

Nürnberg, D. and Müller, R.D., 1991. The tectonic evolution of the South Atlantic from Late Jurassic to present. Tectonophysics, 191(1-2), 27-53.

Nyblade, A.A. and Robinson, S.W., 1994. The African superswell. Geophysical Research Letters, 21(9), 765-768.

Nyblade, A.A. and Sleep, N.H., 2003. Long lasting epeirogenic uplift from mantle plumes and the origin of the southern African Plateau. Geochemistry, Geophysics, Geosystems, 4(12), 1105.

Paton, D.A., van der Spuy, D., di Primio, R. and Horsfield, B., 2008. Tectonically induced adjustment of passive-margin accommodation space; influence on the hydrocarbon potential of the Orange Basin, South Africa. AAPG Bulletin, 92(5), 589-609.

Pedersen, T. and van der Beek, P., 1994. Extension and magmatism in the Oslo Rift, Southeast Norway; no sign of a mantle plume. Earth and Planetary Science Letters, 123(1-4), 317-329.

Reid, D.L., Erlank, A.J. and Rex, D.C., 1991. Age and correlation of the False Bay dolerite dyke swarm, south-western Cape, Cape Province. South African Journal of Geology, 94(2-3), 155-158.

Reid, D.L. and Rex, D.C., 1994. Cretaceous dykes associated with the opening of the South Atlantic; the Mehlberg Dyke, northern Richtersveld. South African Journal of Geology, 97(2), 135-145.

Roberts, A.M., Kusznir, N.J., Yielding, G. and Styles, P., 1998. 2D flexural backstripping of extensional basins; the need for a sideways glance. Petroleum Geoscience, 4(4), 327-338.

Royden, L. and Keen, C.E., 1980. Rifting process and thermal evolution of the continental margin of eastern Canada determined from subsidence curves. Earth and Planetary Science Letters, 51(2), 343-361.

Rutter, E.H., Brodie, K.H. and Evans, P.J., 1993. Structural geometry, lower crustal magmatic underplating and lithospheric stretching in the Ivrea-Verbano zone, northern Italy. Journal of Structural Geology, 15(3-5), 647-662.

Scheck, M. and Bayer, U., 1999. Evolution of the Northeast German Basin -- inferences from a 3D structural model and subsidence analysis. Tectonophysics, 313(1-2), 145-169.

Sclater, J.G. and Christie, P.A.F., 1980. Continental stretching, An explanation of the Post-Mid-Cretaceous subsidence of the central North Sea Basin. Journal of Geophysical Research, 85(B7), 3711-3739.

Seider, G. and Mitchell, J.G., 1976. Episodic Mesozoic volcanism in Namibia and Brazil: A Kr-Ar isochron study bearing on the opening of the South Atlantic. Earth and Planetary Science Letters, 30 292-303.

Shapiro, N.M. and Ritzwoller, M.H., 2004. Inferring surface heat flux distributions guided by a global seismic model, particular application to Antarctica. Earth and Planetary Science Letters, 223(1-2), 213-224.

Stein, C.A. and Stein, S., 1992. A model for the global variation in oceanic depth and heat flow with lithospheric age. Nature (London), 359(6391), 123-129.

Stewart, J., Watts, A.B. and Bagguley, J.G., 2000. Three-dimensional subsidence analysis and gravity modelling of the continental margin offshore Namibia. Geophysical Journal International, 141(3), 724-746.

Talwani, M. and Abreu, V., 2000. Inferences regarding initiation of oceanic crust formation from the U.S. East Coast Margin and conjugate South Atlantic margins. In: W. Mohriac, Talwani, M. (Editor), Atlantic rifts and continental margins. American Geophysical Union, Washington, DC, United States, pp. 211-233.

Thybo, H., Maguire, P.K.H., Birt, C. and Perchuc, E., 2000. Seismic reflectivity and magmatic underplating beneath the Kenya Rift. Geophysical Research Letters, 27(17), 2745-2748.

Tinker, J., de Wit, M. and Brown, R., 2008. Mesozoic exhumation of the southern Cape, South Africa, quantified using apatite fission track thermochronology. Tectonophysics, 455(1-4), 77-93.

van Balen, R.T., van der Beek, P.A. and Cloetingh, S.A.P.L., 1995. The effect of rift shoulder erosion on stratal patterns at passive margins; implications for sequence stratigraphy. Earth and Planetary Science Letters, 134(3-4), 527-544.

van der Spuy, D., 2003. Aptian source rocks in some South Africa Cretaceous basins. In: T. Arthur, MacGregor, D.S., Cameron, N.R. (Editor), Petroleum Geology of Africa: New Themes and Developing Technologies. Geological Society, Special Publications, London, pp. 185-202.

van der Spuy, D., Jikelo, N.A., Ziegler, T. and Bowyer, M., 2003. Deepwater 2D data reveal Orange basin objectives off western South Africa. Oil & Gas Journal, 101, 44-49.

van Wees, J.D. and Beekman, F., 2000. Lithosphere rheology during intraplate basin extension and inversion; inferences from automated modeling of four basins in Western Europe. Tectonophysics, 320(3-4), 219-242.

van Wees, J.D. and Stephenson, R.A., 1995. Quantitative modelling of basin and rheological evolution of the Iberian Basin (Central Spain): implications for lithospheric dynamics of intraplate extension and inversion. Tectonophysics, 252(1-4), 163-178.

van Wees, J.D., Van Bergen, F., David, P., Nepveu, M., Beekman, F., Cloetingh, S., in press. Probabilistic tectonic heat flow modelling for basin maturation: assessment method and applications. Marine and Petroleum Geology.

van Wees, J.D., van Bergen, F., David, P., Nepveu, M., Beekman, F., Cloetingh, S. Probabilistic tectonic heat flow modelling for basin maturation: assessment method and applications, Marine and Petroleum Geology (2009), doi: 10.1016/j.marpetgeo.2009.01.020

van Wijk, J.W., Huismans, R.S., ter Voorde, M. and Cloetingh, S.A.P.L., 2001. Melt generation at volcanic continental margins; no need for a mantle plume? Geophysical Research Letters, 28(20), 3995-3998.

Watts, A.B. and Fairhead, J.D., 1999. A process-oriented approach to modeling the gravity signature of continental margins. The Leading Edge, 18, 258-263.

White, R. and McKenzie, D., 1989. Magmatism at rift zones - The generation of volcanic continental margins and flood basalts. Journal of Geophysical Research, 94(6), 7685-7729.

Wilson, M., 1993. Magmatism and the geodynamics of basin formation. Sedimentary Geology, 86(1-2), 5-29.

Figure captions

Figure 1: a) Simplified geological map of southwestern Africa (modified after de Wit and Stankiewitz, 2007). b) Location map of the Orange Basin with isopach distribution of postrift strata indicating the main depocentre and major tectonic elements (after Jungslager, 1999 in Paton et al. 2008). c) Bathymetric map of the working area offshore west South Africa. The black line outlines the area covered by the model presented in this study, overlain by yellow lines indicating the position of available seismic lines which are embraced by a blue line marking the area of best data coverage. Black diamonds represent the analysed wells. The orange line documents the position of the cross-section shown in Figure 3.

Figure 2: a) WSW-ENE oriented profile through the working area (for position see Figure 1) illustrating the main features of the margin comprising sequence stratigraphic boundaries (after Brown et al., 1995). Additionally, the positions of the wells are projected along the transect. TWT=two-way travel time. b) Line drawing of the profile with the megasequences modified after Paton et al. (2008) and the depth levels of potential source rock interval (indicated by black stars).

Figure 3: Stratigraphy of seismic reflections and ages of previous studies (Brown et al., 1995) between the analysed individual wells with the according lithologies. Red stars indicate the location and age of potential source rock intervals (Brown et al., 1995). MA = Maastrichtian, CA = Campanian, SA = Santonian, CO = Coniacian, TU = Turonian, CE = Cenomanian, AL = Albian, AP = Aptian, BA = Barremian, HA = Hauterivian, VA = Valanginian, BE = Berriasian, Ma = age in million of years using the timescale of Haq et al. (1988).

Figure 4: a) Thickness map of the high velocity, high density body modelled by Hirsch et al. (2007) which is used in this study. b)Thickness map of the syn-rift succession derived from seismic interpretation.

Figure 5: Thickness maps of the main sedimentary sequences for different time intervals derived from seismic interpretation.

Figure 6: Maps indicating the amount of eroded material across the working area as derived from seismic interpretation a) amount of removed sediments between 74-67 Ma, b) sediments which were removed between 16 and 14 Ma.

Figure 7: a) Tectonic subsidence curves derived by backstripping the wells. b) Plot of the according forward models that fit the observed tectonic subsidence best.

Figure 8: a) Subsidence curves for well A-C1: in green is the basement and in blue the tectonic subsidence curve shown. The latter is overlain by the tectonic subsidence curve predicted by the best-fit forward model. The light blue curve documents the paleo water depth distribution used throughout the modelling for well A-C1. b) Forward models for well A-C1. Whereas the red curve obeys the rules of a uniform stretching model (McKenzie, 1978) and considers only uniform stretching, the green curve represents a forward model which incorporates the emplacement of underplating in the syn-rift stage. The blue curve stands for a model which accounts for underplating and also mantle stretching from 74 Ma on.

Figure 9: Heat flow evolution (in red) and development of the lithospheric thickness (in blue) for well A-C1 compared for two models: Solid lines indicate the uniform stretching model (McKenzie, 1978) whereas dashed lines represent the best fit forward model including departures from the uniform stretching model such as underplating and post-rift stretching of the lithospheric mantle.

Figure 10: Evolution of the lithospheric thickness through time for all backstripped wells as predicted by the best-fit forward models.

Figure 11: a) Comparison of the vitrinite reflectance profiles as predicted by the forward models to the measured maturity of each well. b) Comparison of the vitrinite reflectance as predicted by the forward models if more erosion is assumed as predicted by seismic interpretation to the measured maturity of each well.

Figure 12: Illustration of the lateral variations of the tectonic subsidence along two representative transects through the basin. Each diagram depicts the tectonic subsidence curve of a synthetic well and colours indicate the position of the well along the transect. a) Tectonic subsidence curves for synthetic wells along the north-south running profile on the shelf and b) along a line which transects the basin in east-west direction.

Figure 13: The distribution of effective crustal stretching values across the working area which varies between 1.0 close to the coast and 2.2 in the distal parts of the model. Red points indicate the position of the real wells and the calculated stretching factor for each well. Each coloured square represents one of the synthetic wells. The white mask outlines the area best constrained by seismic data.

Figure 14: Map view of the increase of tectonic subsidence for several time steps. Details are given in the text.

Figure 15: Spatial distribution of the temperature within the Barremian/Aptian source rock interval at 74 Ma.

Figure 16: a) Spatial distribution of the required stretching factors of the lithospheric mantle between 74 and 67 Ma. b) Thickness map of the lithosphere at 67 Ma in consequence of renewed stretching.

Figure 17: a) Map view of the calculated uplift across the margin documenting the pure tectonically induce vertical movement of the basin from 74 to 67 Ma. b) Map view of the increase in basement heat flow coeval to margin uplift between 74 and 67 Ma.

Figure 18: Map of the predicted temperature distribution within the Barremian /Aptian source rock at 16 Ma.

Figure 19: Map illustrating the spatial distribution of stretching factors for the lithospheric mantle for the time interval from 16 to 14 Ma.

Figure 20: a) Map view of the calculated tectonically induced uplift for the time interval from 16 to 14 Ma indicating that maximum uplift occurred in the NW of the model. b) Map view of the increase in basement heat flow from 16 to 14 Ma.

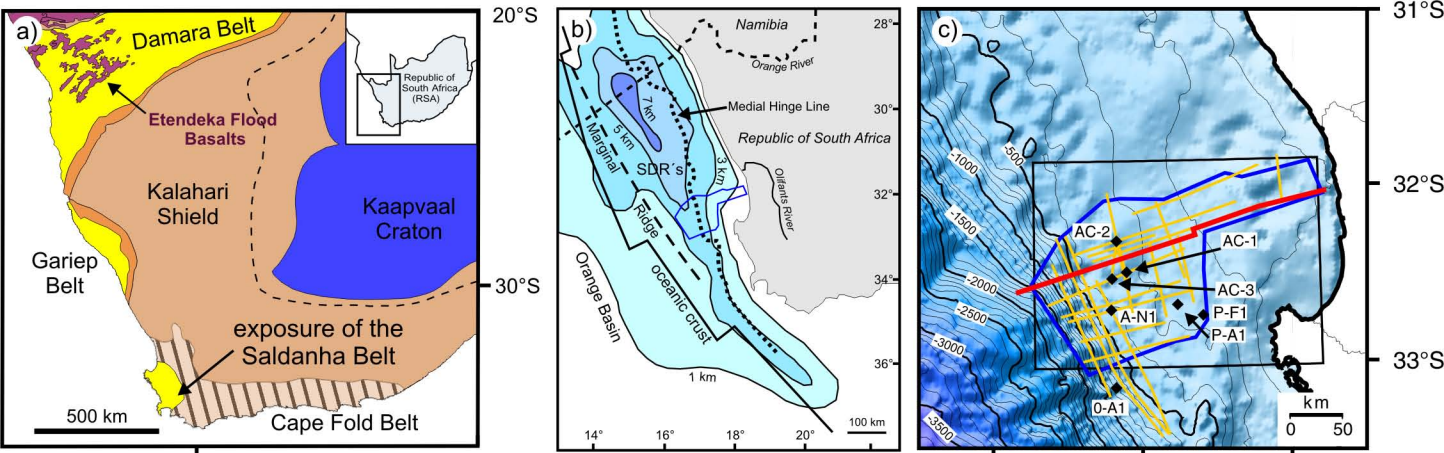
a)
Damara Belt
Republic of South Africa (RSA)
Etendeka Flood Basalts
Kalahari Shield
Kaapvaal Craton
Gariep Belt
exposure of the Saldanha Belt
Cape Fold Belt
500 km
20°S
30°S
20°E
30°E
b)
Namibia
Orange River
Medial Hinge Line
Republic of South Africa
7 km
5 km
3 km
Marginal
SDR´s
Ridge
oceanic crust
Olifants River
Orange Basin
1 km
100 km
28°
30°
32°
34°
36°
14°
16°
18°
20°
c)
-500
-1000
-1500
-2000
-2500
-3000
-3500
AC-2
AC-1
AC-3
A-N1
P-F1
P-A1
0-A1
km
0
50
31°S
32°S
33°S
16°E
17°E
18°E
Cretaceous igneous intrusions
Late Paleozoic-Mesozoic
Neoproterozoic Juvenile
Meso/Paleoproterozoic
Neoproterozoic remobilised Proterozoic
Archaean
SDR Seaward-dipping reflector

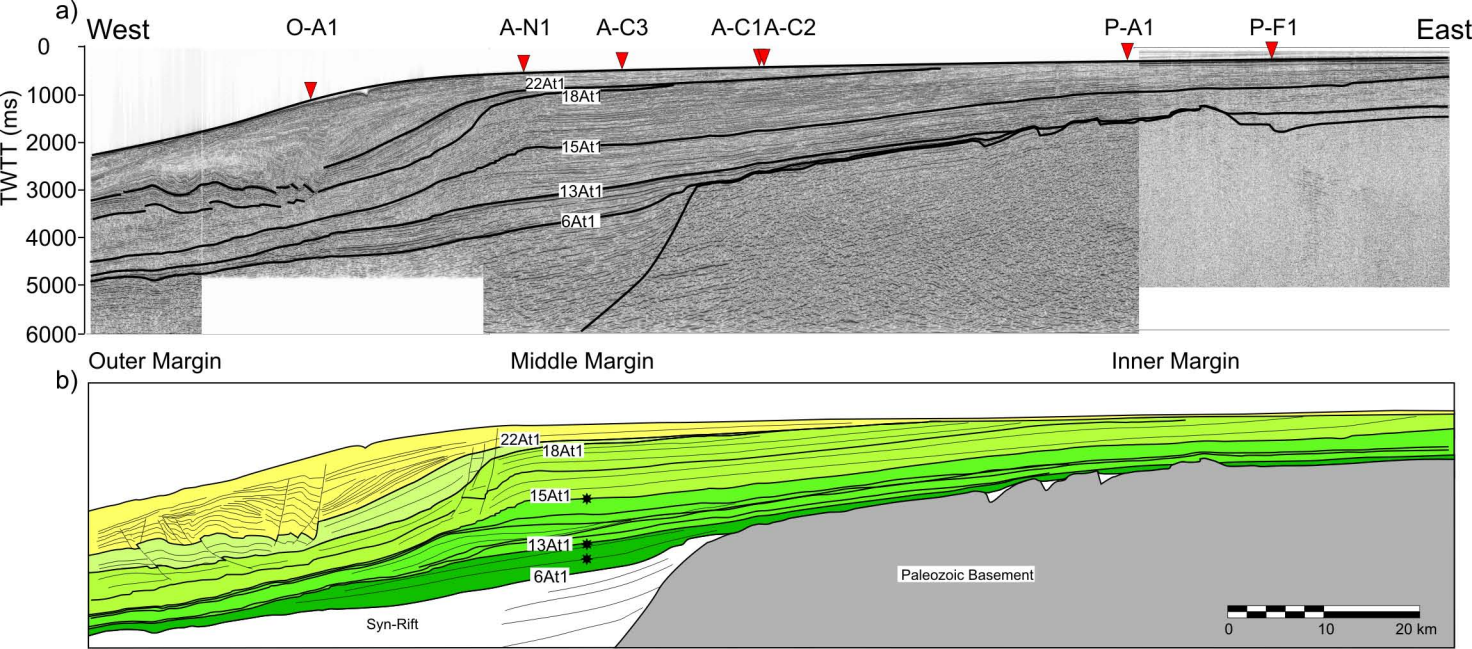
a)
West
O-A1
A-N1
A-C3
A-C1A-C2
P-A1
P-F1
East
TWTT (ms)
0
1000
2000
3000
4000
5000
6000
22At1
18At1
15At1
13At1
6At1
Outer Margin
Middle Margin
Inner Margin
b)
22At1
18At1
15At1
13At1
6At1
Paleozoic Basement
Syn-Rift
0
10
20 km

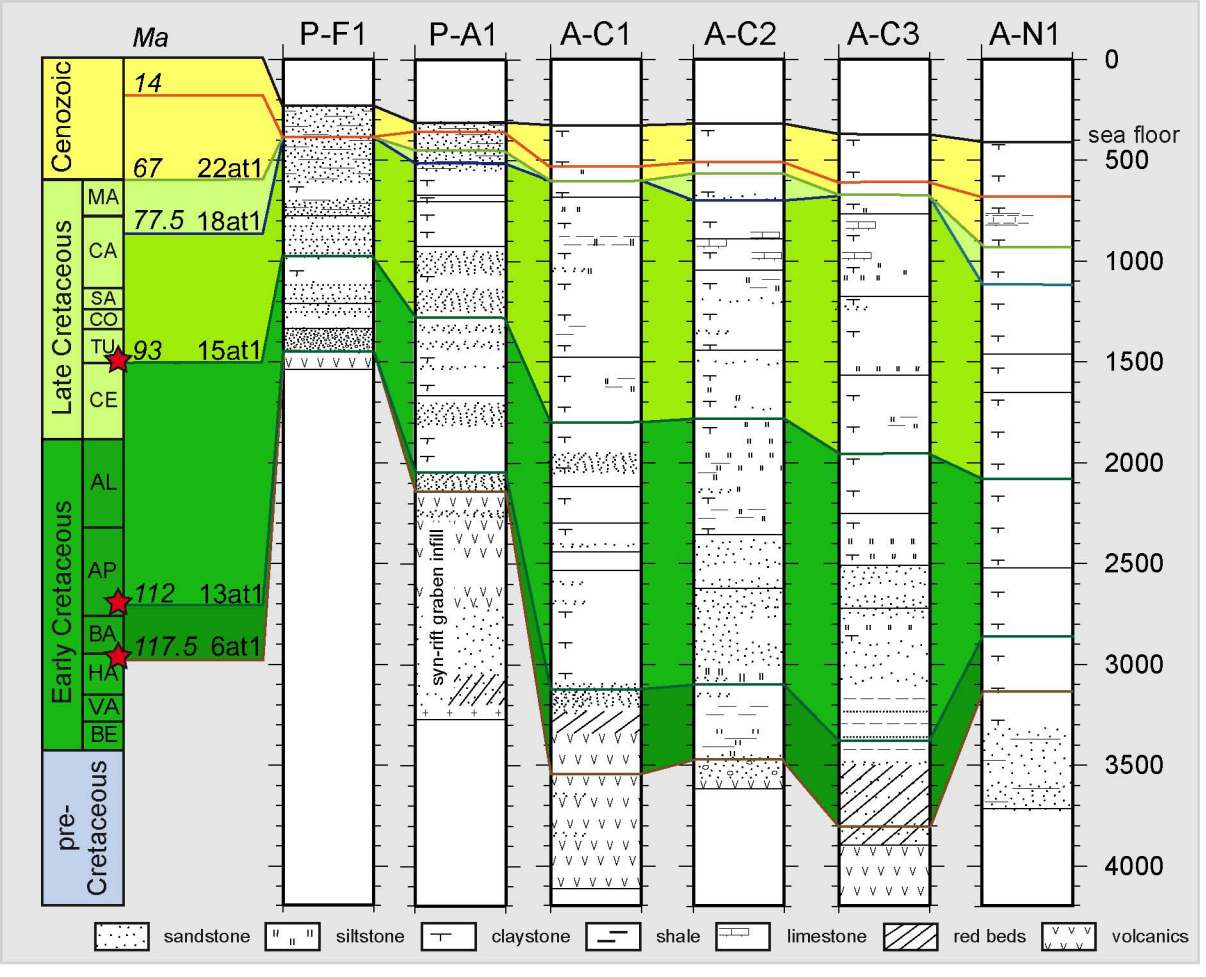
Ma
P-F1
P-A1
A-C1
A-C2
A-C3
A-N1
Cenozoic
Late Cretaceous
Early Cretaceous
pre-Cretaceous
MA
CA
SA
CO
TU
CE
AL
AP
BA
HA
VA
BE
14
67
22at1
77.5
18at1
93
15at1
112
13at1
117.5
6at1
syn-rift graben infill
0
sea floor
500
1000
1500
2000
2500
3000
3500
4000
sandstone
siltstone
claystone
shale
limestone
red beds
volcanics

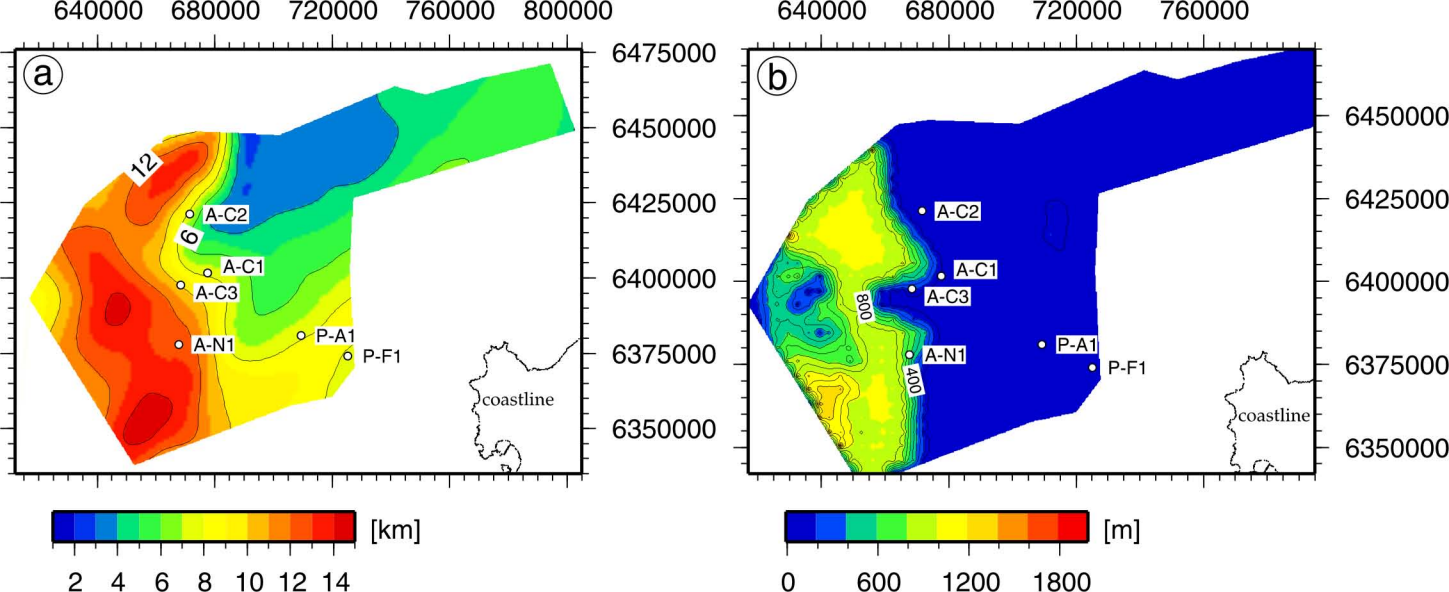
640000
680000
720000
760000
800000
a
12
6
A-C2
A-C1
A-C3
A-N1
P-A1
P-F1
coastline
6475000
6450000
6425000
6400000
6375000
6350000
[km]
2 4 6 8 10 12 14
640000
680000
720000
760000
b
800
400
A-C2
A-C1
A-C3
A-N1
P-A1
P-F1
coastline
6450000
6425000
6400000
6375000
6350000
[m]
0 600 1200 1800

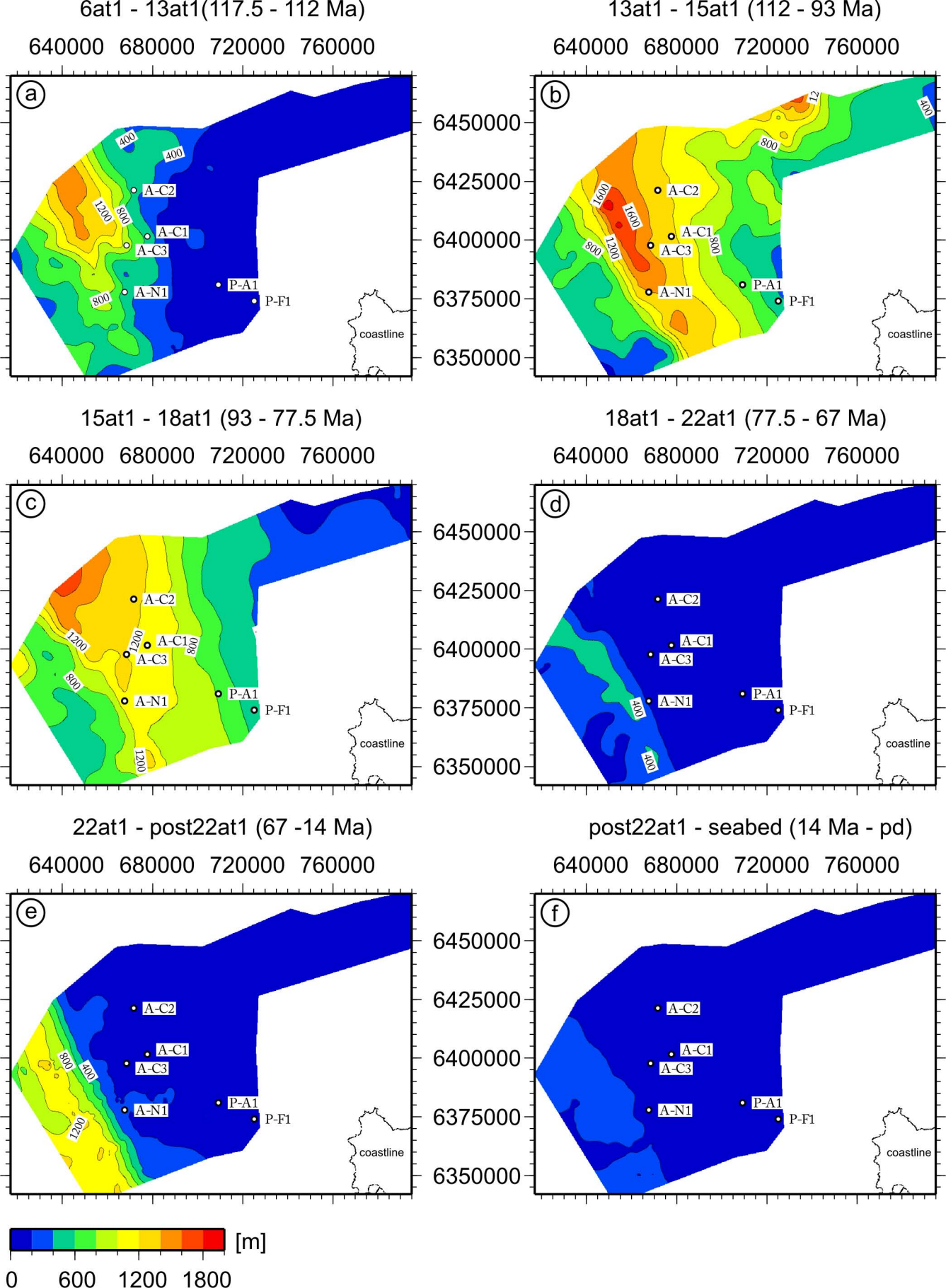
6at1 - 13at1(117.5 - 112 Ma)
13at1 - 15at1 (112 - 93 Ma)
15at1 - 18at1 (93 - 77.5 Ma)
18at1 - 22at1 (77.5 - 67 Ma)
22at1 - post22at1 (67 -14 Ma)
post22at1 - seabed (14 Ma - pd)
640000 680000 720000 760000
6450000
6425000
6400000
6375000
6350000
a
b
c
d
e
f
A-C2
A-C1
A-C3
A-N1
P-A1
P-F1
coastline
400
800
1200
1600
[m]
0 600 1200 1800

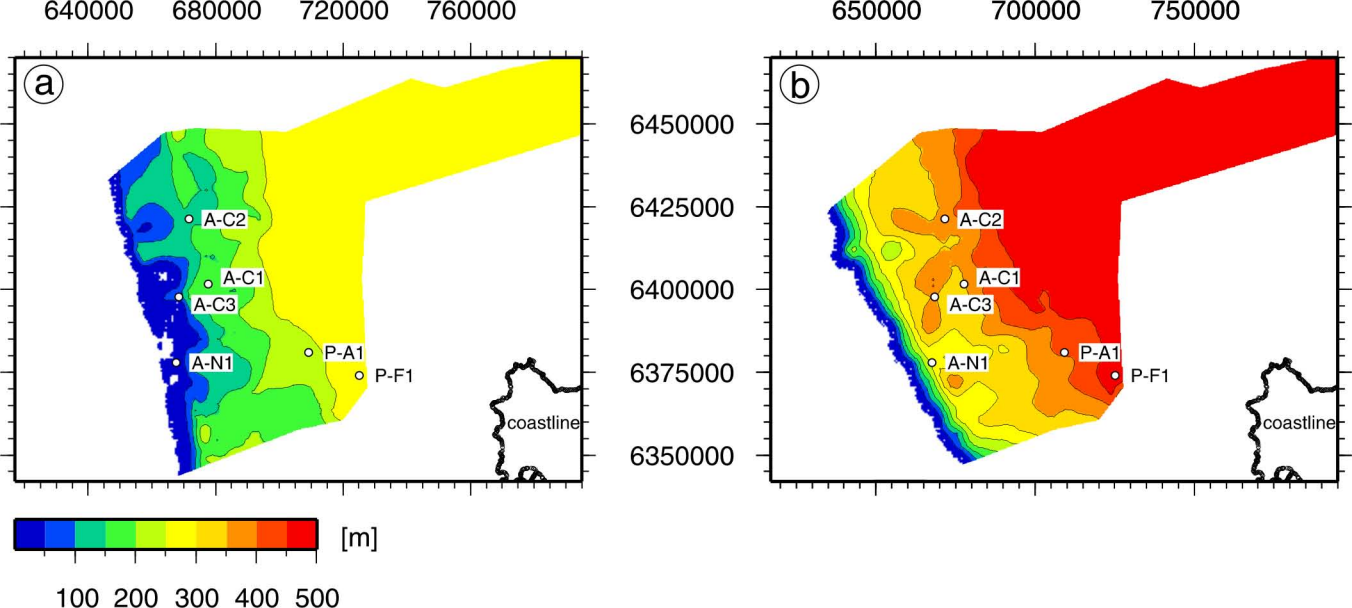
640000
680000
720000
760000
650000
700000
750000
a
b
6450000
6425000
6400000
6375000
6350000
A-C2
A-C1
A-C3
A-N1
P-A1
P-F1
coastline
[m]
100 200 300 400 500

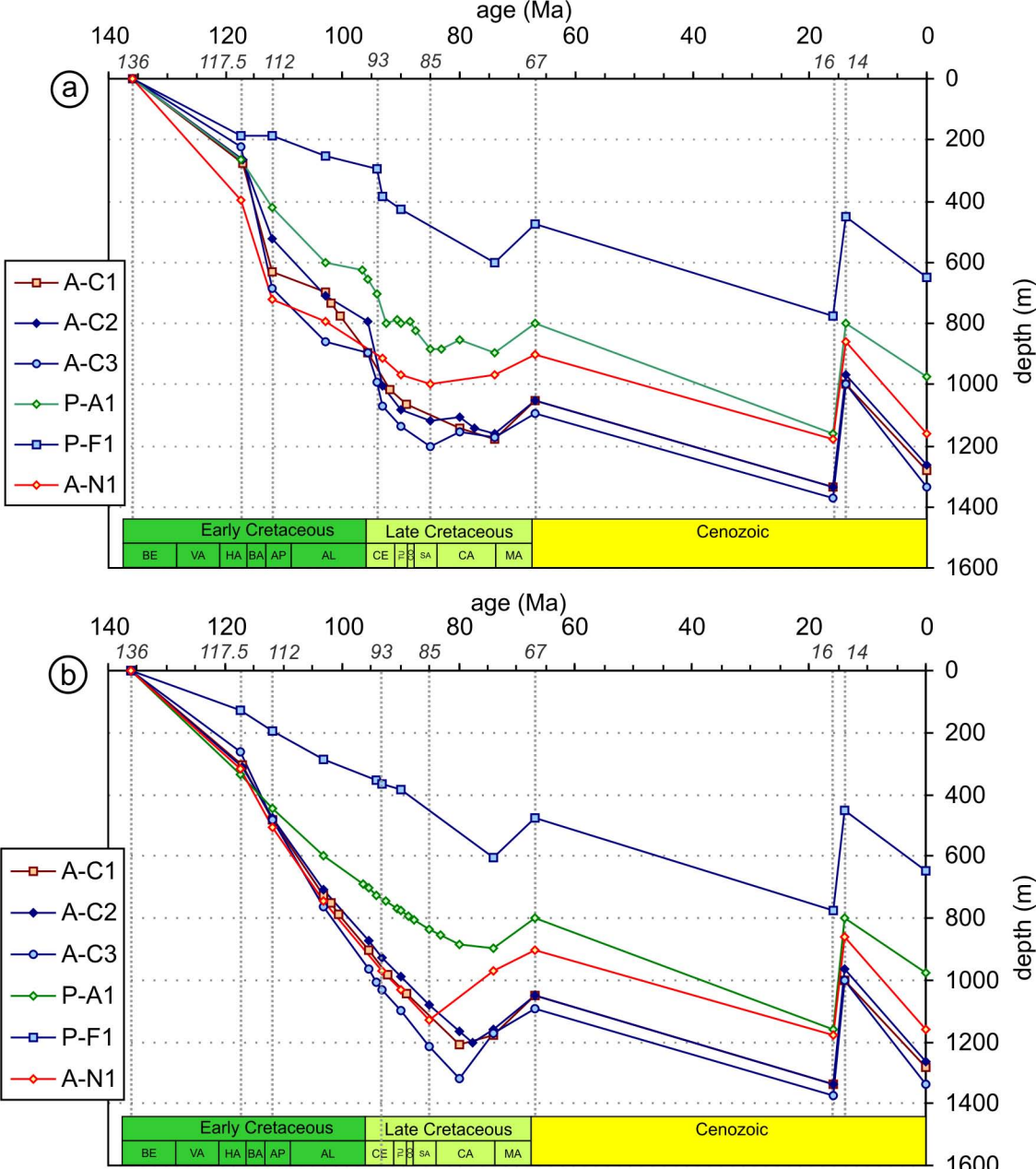
a
b
age (Ma)
140
120
100
80
60
40
20
0
136
117.5
112
93
85
67
16
14
depth (m)
0
200
400
600
800
1000
1200
1400
1600
A-C1
A-C2
A-C3
P-A1
P-F1
A-N1
Early Cretaceous
Late Cretaceous
Cenozoic
BE
VA
HA
BA
AP
AL
CE
SA
CA
MA

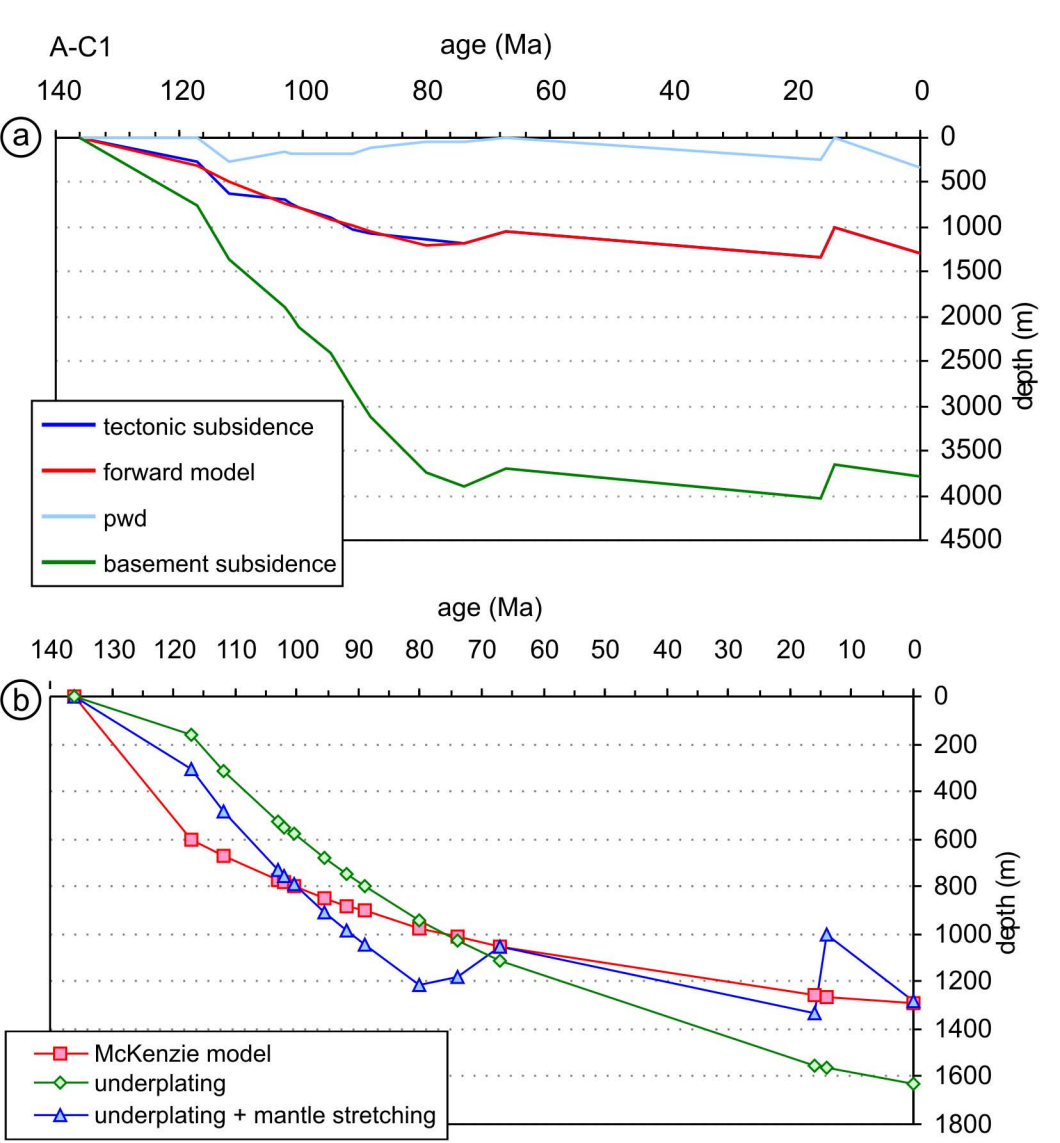
A-C1
age (Ma)
140
120
100
80
60
40
20
0
a
0
500
1000
1500
2000
2500
3000
3500
4000
4500
depth (m)
tectonic subsidence
forward model
pwd
basement subsidence
age (Ma)
140
130
120
110
100
90
80
70
60
50
40
30
20
10
0
b
0
200
400
600
800
1000
1200
1400
1600
1800
depth (m)
McKenzie model
underplating
underplating + mantle stretching

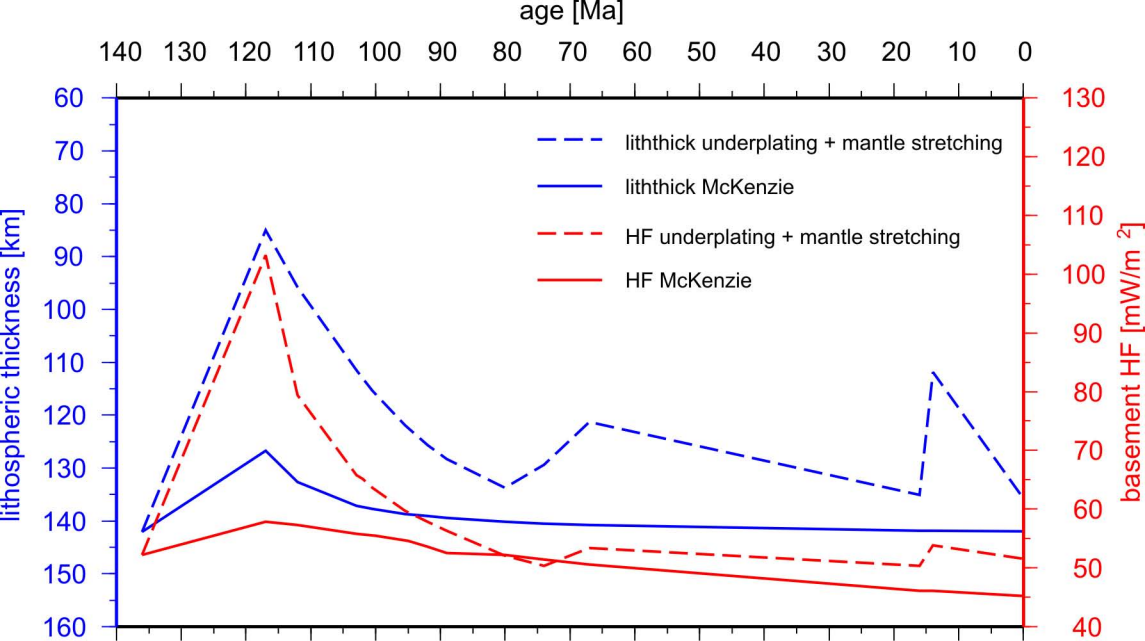
age [Ma]
140 130 120 110 100 90 80 70 60 50 40 30 20 10 0
lithospheric thickness [km]
60 70 80 90 100 110 120 130 140 150 160
basement HF [mW/m 2]
130 120 110 100 90 80 70 60 50 40
liththick underplating + mantle stretching
liththick McKenzie
HF underplating + mantle stretching
HF McKenzie

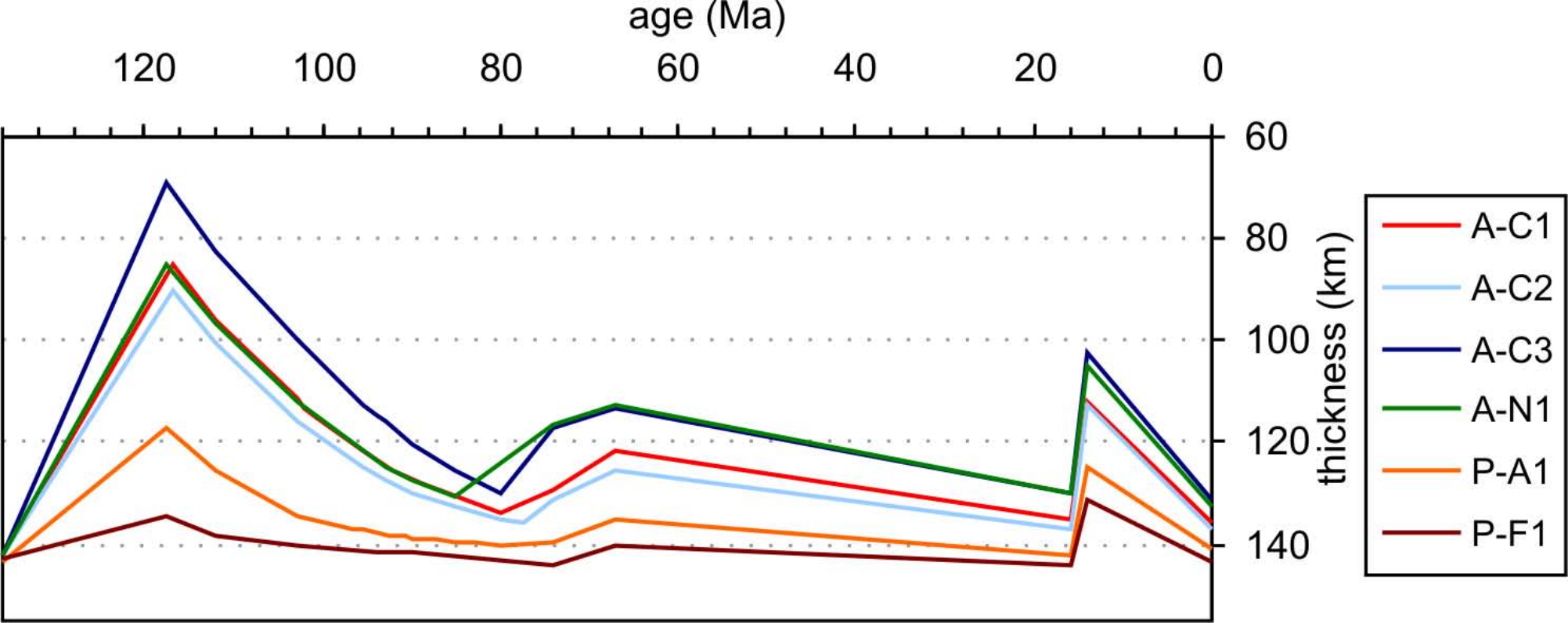
age (Ma)
120
100
80
60
40
20
0
60
80
100
120
140
thickness (km)
A-C1
A-C2
A-C3
A-N1
P-A1
P-F1

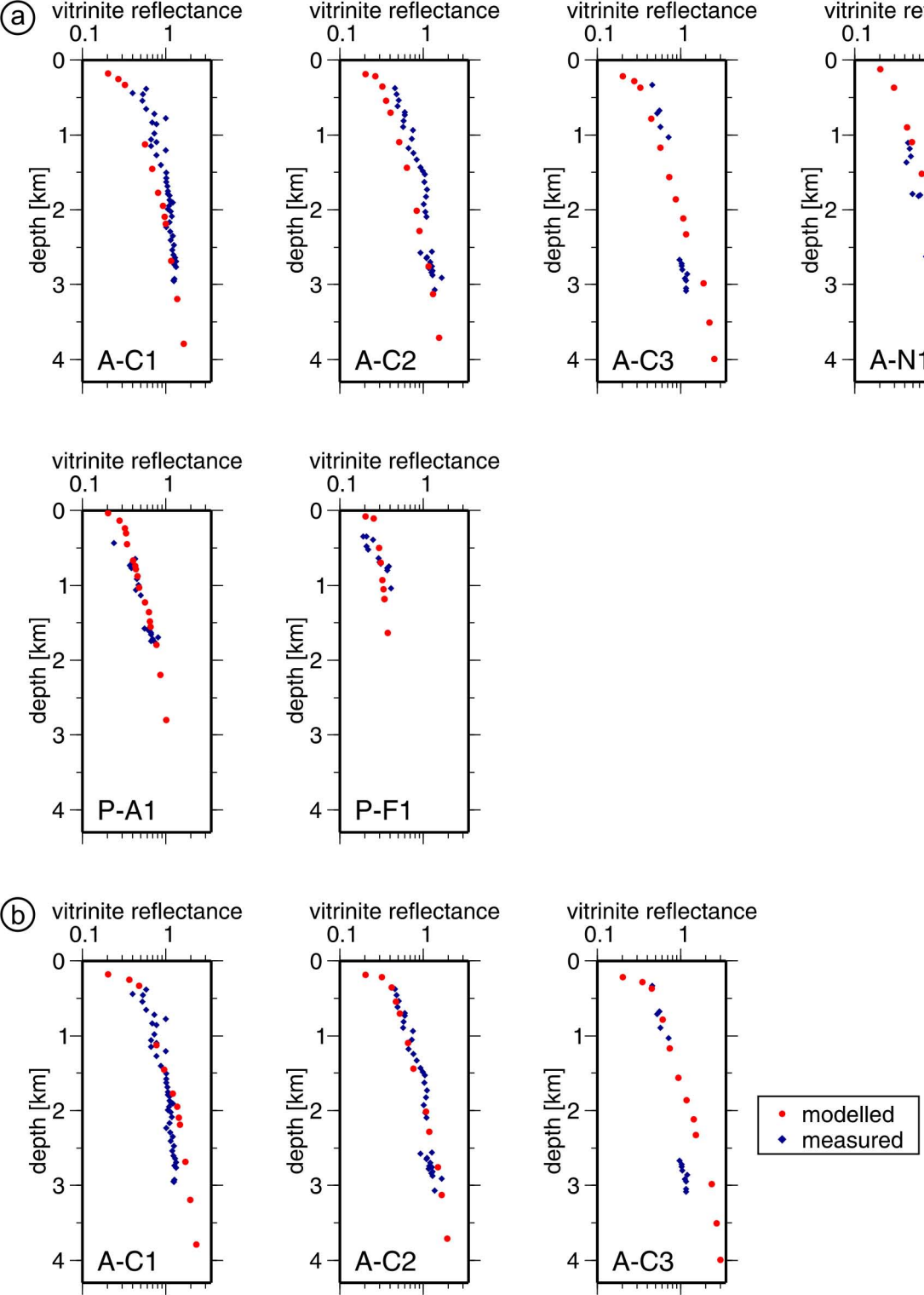
a
vitrinite reflectance
0.1
1
depth [km]
0
1
2
3
4
A-C1
A-C2
A-C3
A-N1
P-A1
P-F1
b
modelled
measured

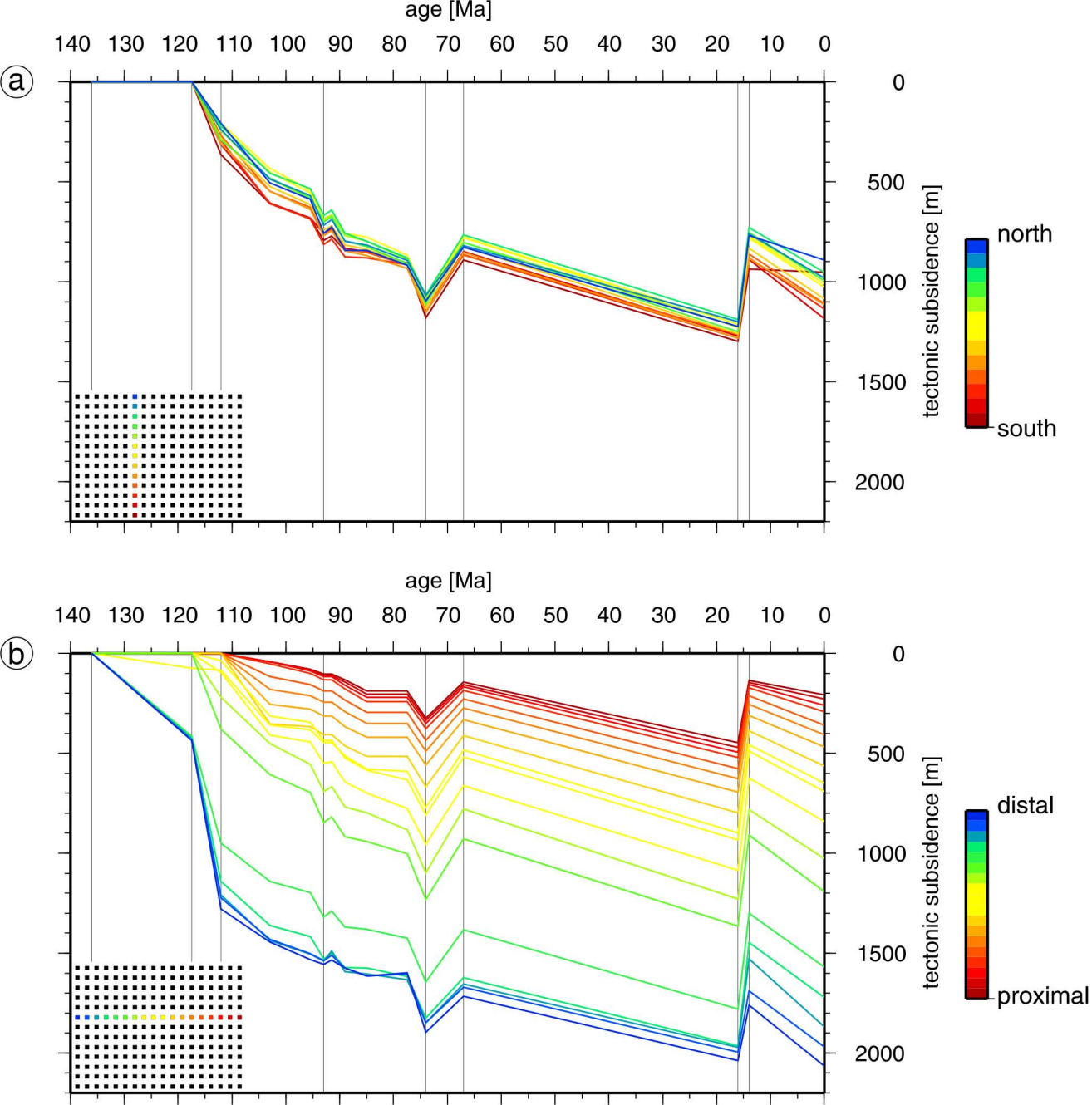
a
age [Ma]
140 130 120 110 100 90 80 70 60 50 40 30 20 10 0
0
500
1000
1500
2000
tectonic subsidence [m]
north
south
b
age [Ma]
140 130 120 110 100 90 80 70 60 50 40 30 20 10 0
0
500
1000
1500
2000
tectonic subsidence [m]
distal
proximal

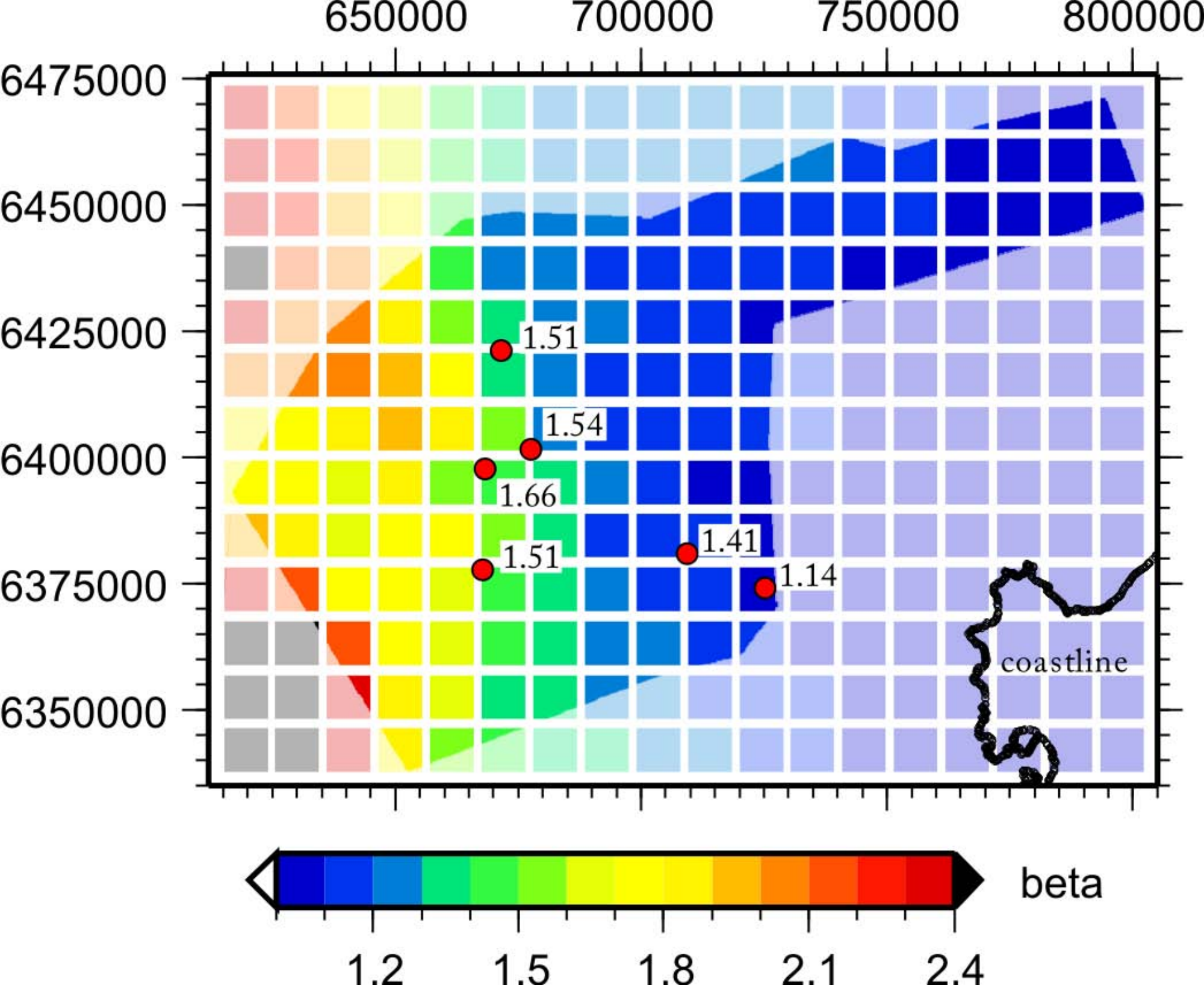
650000
700000
750000
800000
6475000
6450000
6425000
6400000
6375000
6350000
1.51
1.54
1.66
1.41
1.51
1.14
coastline
beta
1.2
1.5
1.8
2.1
2.4

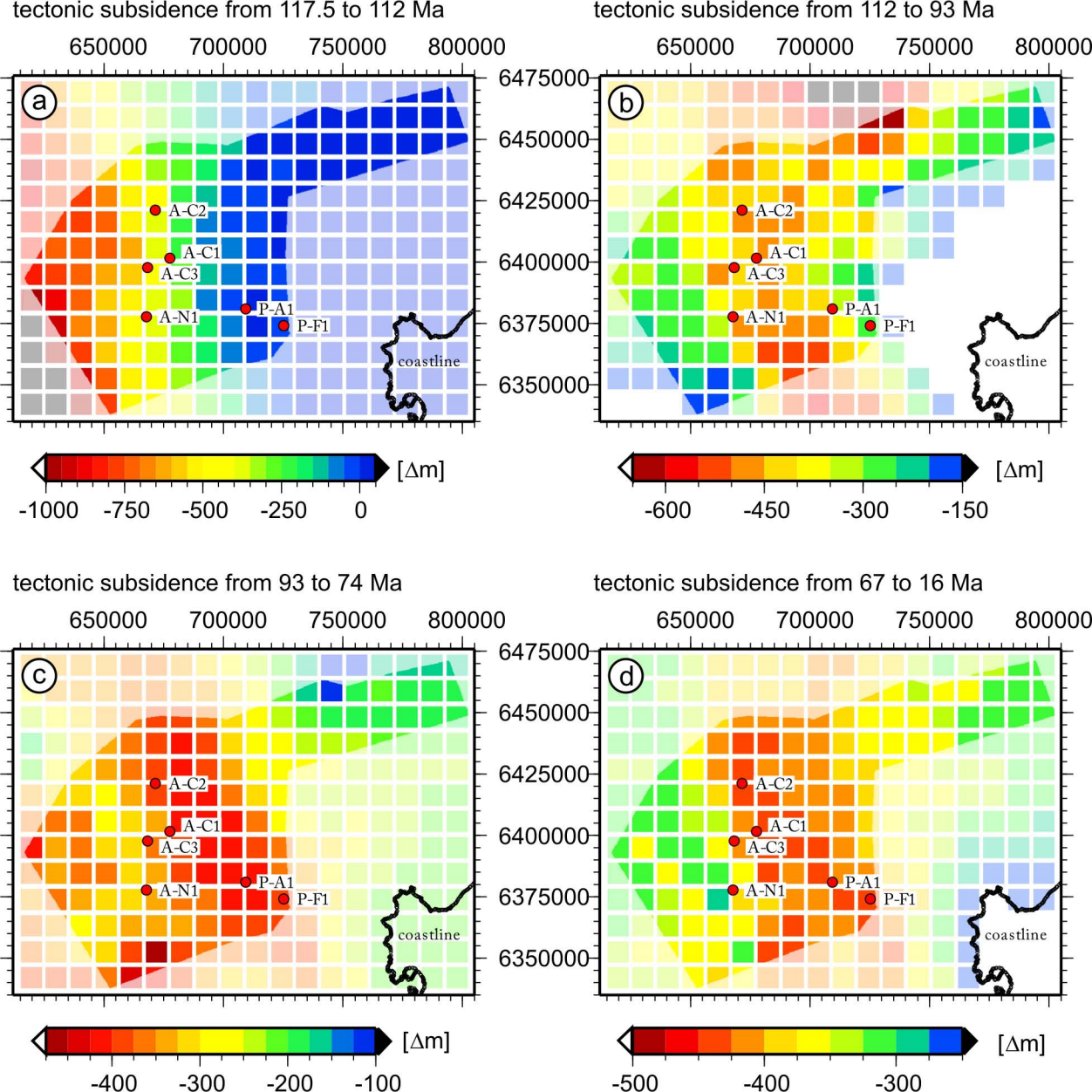
tectonic subsidence from 117.5 to 112 Ma
tectonic subsidence from 112 to 93 Ma
tectonic subsidence from 93 to 74 Ma
tectonic subsidence from 67 to 16 Ma
650000
700000
750000
800000
6475000
6450000
6425000
6400000
6375000
6350000
a
b
c
d
A-C2
A-C1
A-C3
A-N1
P-A1
P-F1
coastline
[Δm]
-1000
-750
-500
-250
0
-600
-450
-300
-150
-400
-200
-100
-500

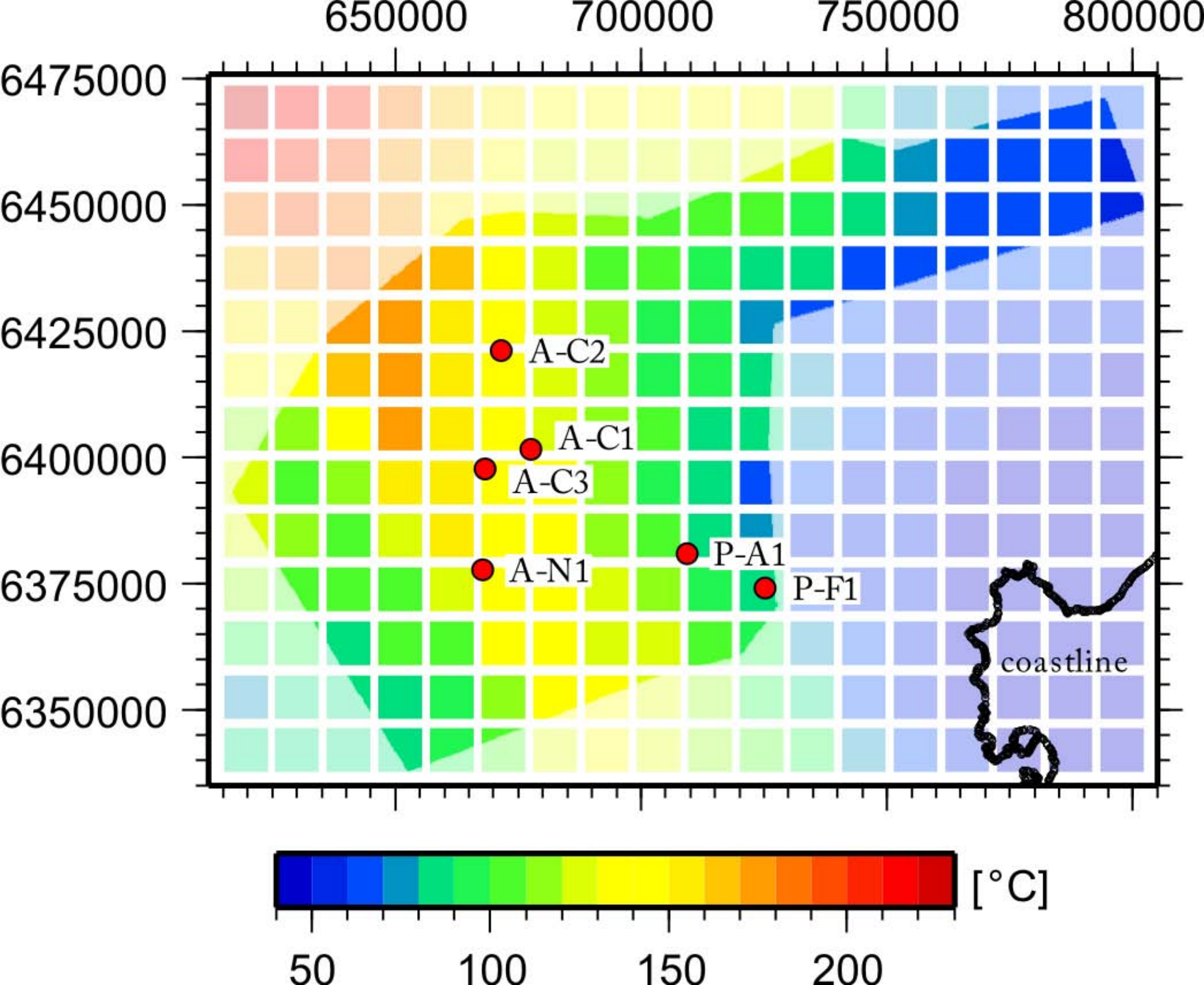
650000
700000
750000
800000
6475000
6450000
6425000
6400000
6375000
6350000
A-C2
A-C1
A-C3
A-N1
P-A1
P-F1
coastline
50
100
150
200
[°C]

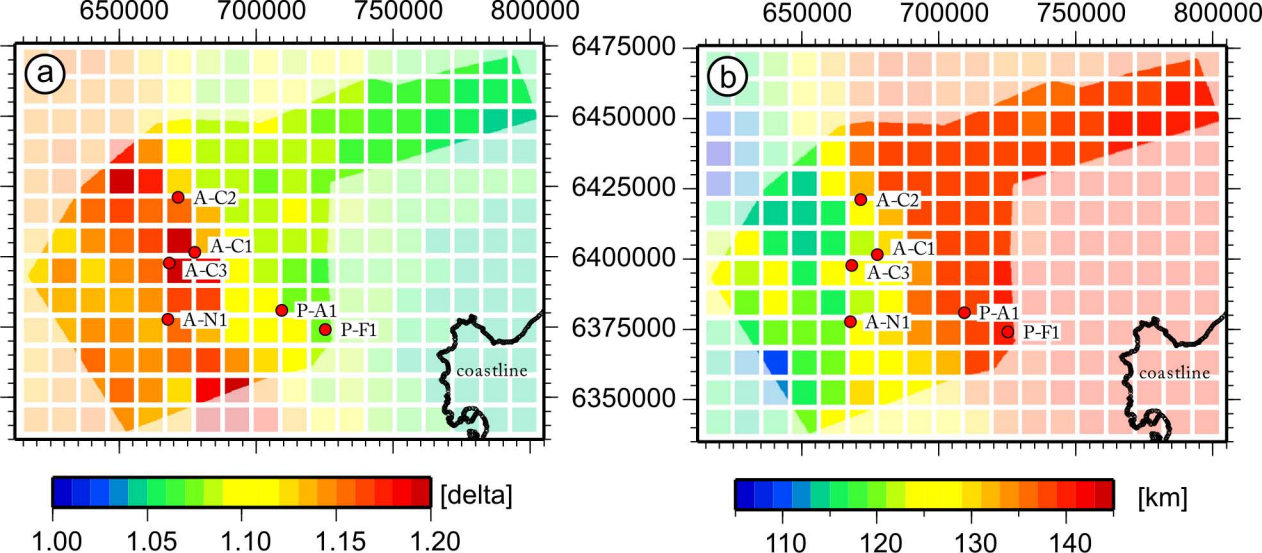
650000
700000
750000
800000
a
A-C2
A-C1
A-C3
A-N1
P-A1
P-F1
coastline
[delta]
1.00
1.05
1.10
1.15
1.20
6475000
6450000
6425000
6400000
6375000
6350000
b
[km]
110
120
130
140

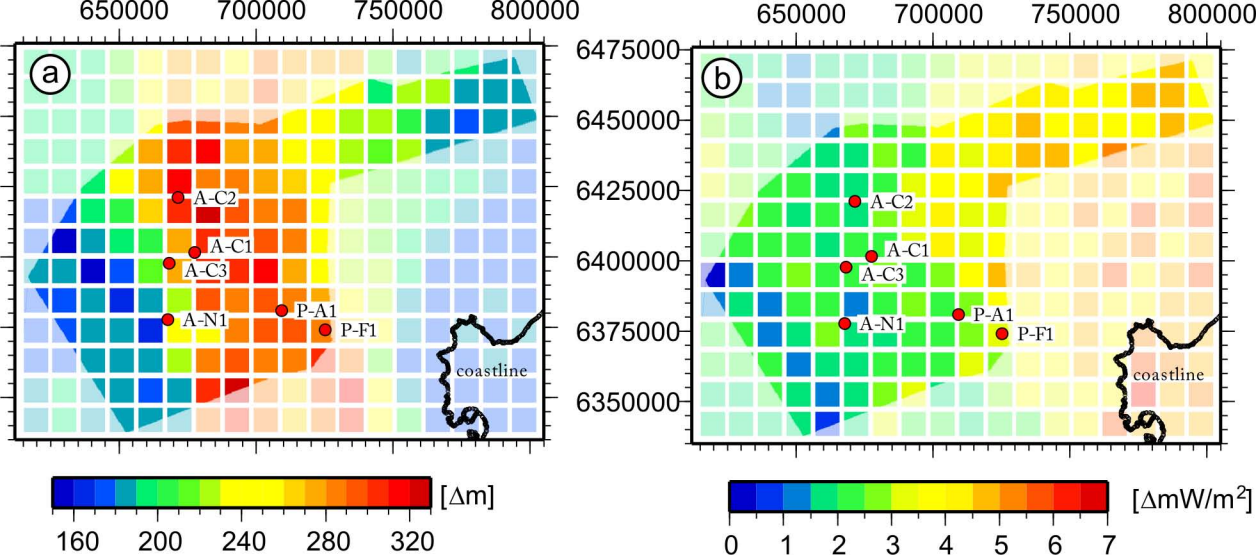
650000
700000
750000
800000
a
A-C2
A-C1
A-C3
A-N1
P-A1
P-F1
coastline
[Δm]
160
200
240
280
320
b
6475000
6450000
6425000
6400000
6375000
6350000
[ΔmW/m²]
0
1
2
3
4
5
6
7

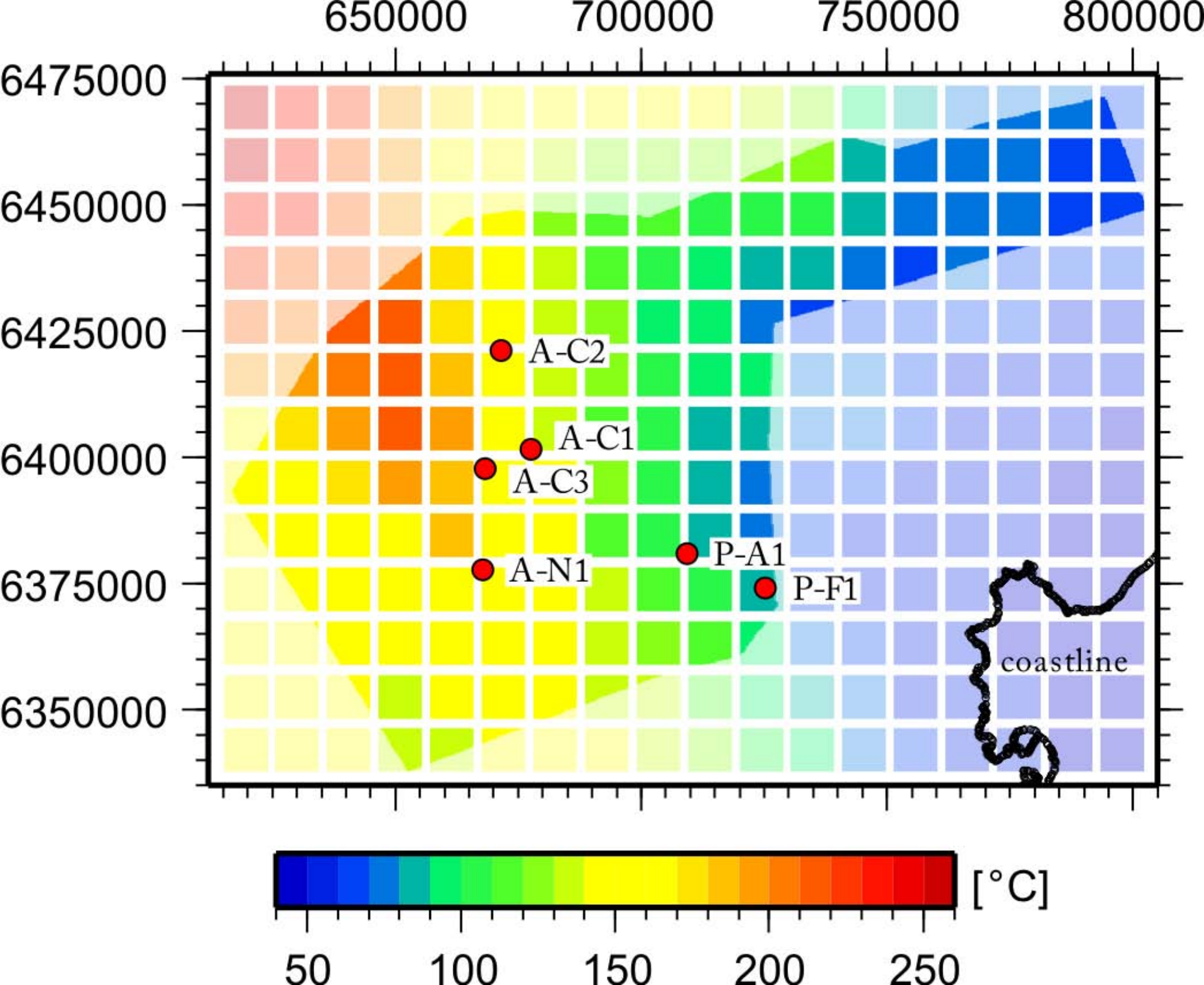
650000
700000
750000
800000
6475000
6450000
6425000
6400000
6375000
6350000
A-C2
A-C1
A-C3
A-N1
P-A1
P-F1
coastline
50
100
150
200
250
[°C]

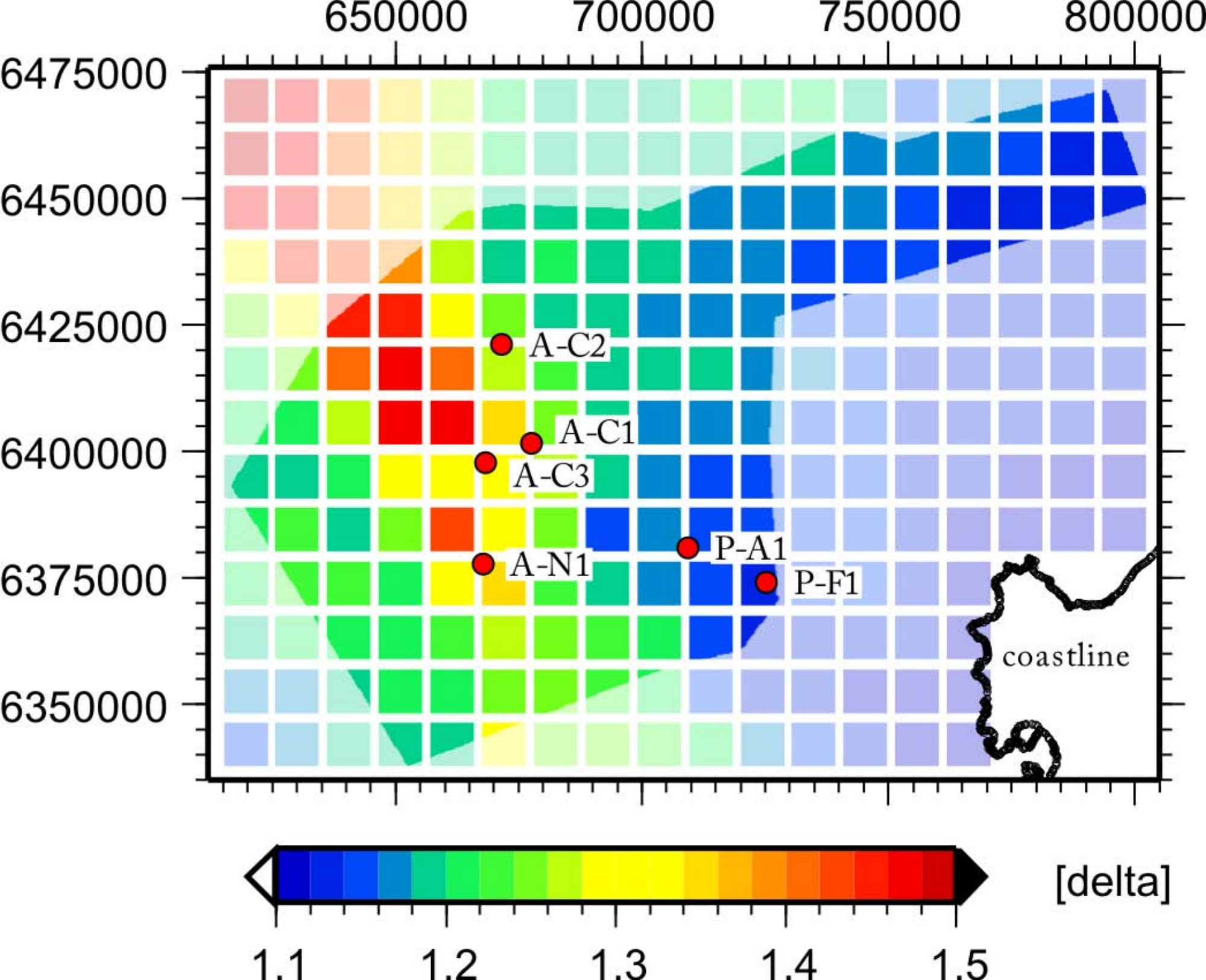
650000
700000
750000
800000
6475000
6450000
6425000
6400000
6375000
6350000
A-C2
A-C1
A-C3
A-N1
P-A1
P-F1
coastline
[delta]
1.1
1.2
1.3
1.4
1.5

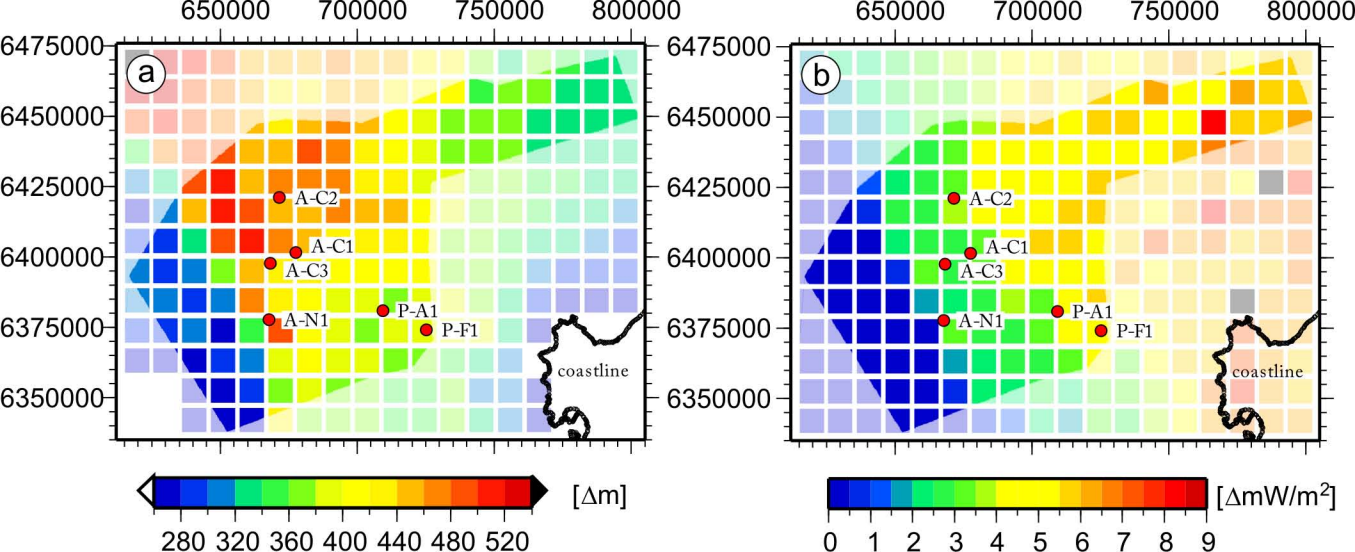
650000
700000
750000
800000
6475000
6450000
6425000
6400000
6375000
6350000
a
A-C2
A-C1
A-C3
A-N1
P-A1
P-F1
coastline
[Δm]
280 320 360 400 440 480 520
b
A-C2
A-C1
A-C3
A-N1
P-A1
P-F1
coastline
[ΔmW/m²]
0 1 2 3 4 5 6 7 8 9

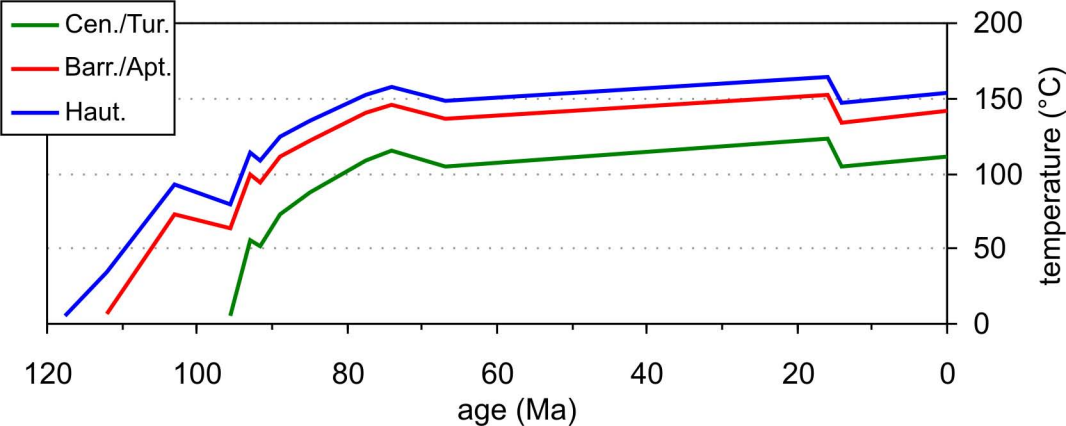
Cen./Tur.
Barr./Apt.
Haut.
200
150
100
50
0
temperature (°C)
120
100
80
60
40
20
0
age (Ma)

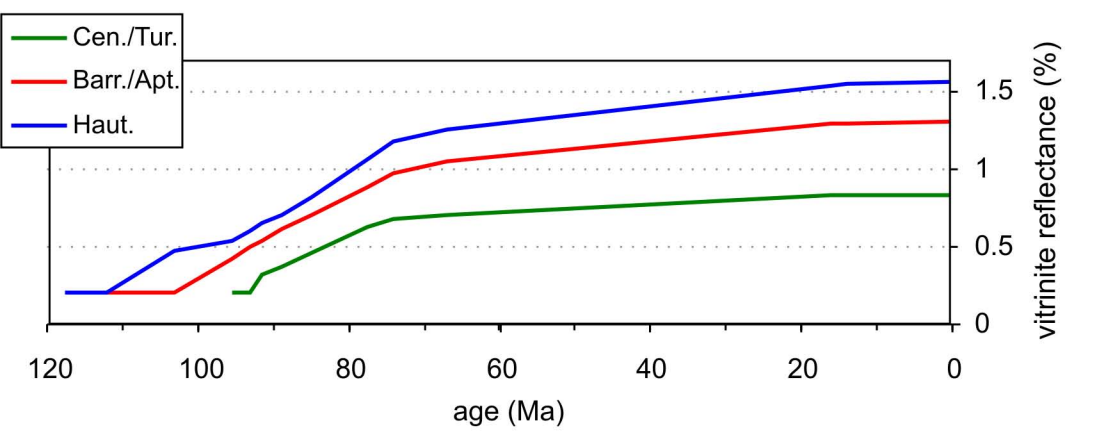
Cen./Tur.
Barr./Apt.
Haut.
1.5
1
0.5
0
vitrinite reflectance (%)
120
100
80
60
40
20
0
age (Ma)

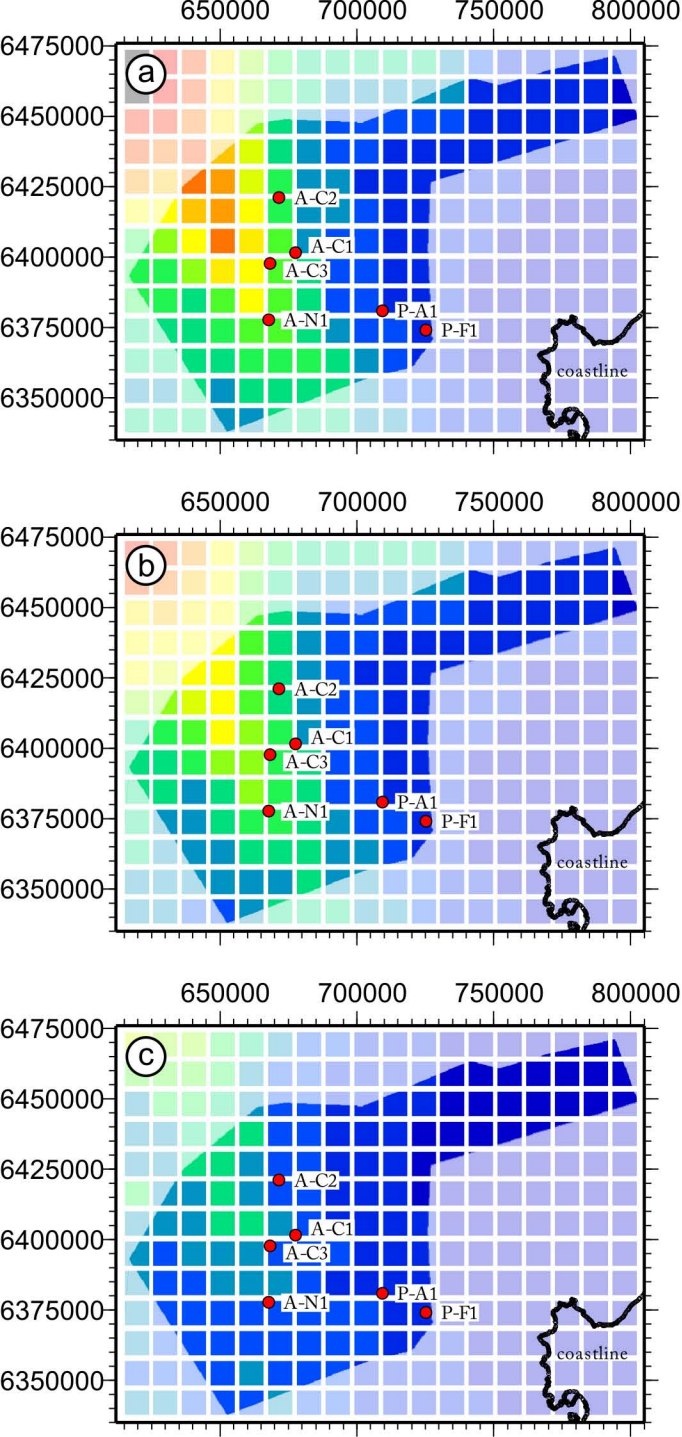
650000
700000
750000
800000
6475000
6450000
6425000
6400000
6375000
6350000
a
A-C2
A-C1
A-C3
A-N1
P-A1
P-F1
coastline
b
c
R0 [%]
3.6
3.0
2.4
1.8
1.2
0.6

ⓐ

model parameter	units	value
initial lithospheric thickness	[km]	146
initial crustal thickness	[km]	36
surface crustal density	[kg/m³]	2900
surface mantle density	[kg/m³]	3300
surface density underplate	[kg/m³]	3000
crustal conductivity	[-]	2.6
mantle conductivity	[-]	3
heat production in the upper crust	[microW/m³]	depends
heat production in the lower crust	[microW/m³]	0.5
lithosphere thermal expansion	[-]	3.50E-05
base lithosphere temperature	[°C]	1330

ⓑ

	ϕ_0	zscale	zscale change	zscale 2
sandstone	35	2300	1000	2000
shale	68	1500	500	1500
silt	50	1800	1000	2000
limestone	50	1400	500	2000

Upper part: $\varphi(z)\big|_{z<=zscalechange} = \varphi_0 e^{-\frac{z}{zscale}}$

Lower part: $\varphi(z)\big|_{z>zscalechange} = \left(\varphi_0 \frac{e^{-\frac{zscalechange}{zscale}}}{e^{-\frac{zscalechange}{zscale2}}} \right) e^{-\frac{z}{scale2}}$

event	A-C1			A-C2			A-C3			A-N1			P-A1			P-F1		
	$\beta_{eff.}$	δ	uplift [m]	$\beta_{eff.}$	δ	uplift [m]	$\beta_{eff.}$	δ	uplift [m]	$\beta_{eff.}$	δ	uplift [m]	$\beta_{eff.}$	δ	uplift [m]	$\beta_{eff.}$	δ	uplift [m]
rifting	1.54			1.51			1.66			1.51			1.41			1.14		
74-67 Ma		1.13	132		1.06	112		1.04	80		1.04	68		1.04	100		1.03	125
16-14 Ma		1.26	345		1.27	379		1.34	388		1.30	317		1.18	367		1.13	325